

**Semiconductor-type SnO₂-based NO₂ sensors operated at room temperature
under UV-light irradiation**

Takeo Hyodo*, Kaoru Urata, Kai Kamada, Taro Ueda, and Yasuhiro Shimizu

Graduate School of Engineering, Nagasaki University
1-14 Bunkyo-machi, Nagasaki 852-8521, Japan

*Corresponding author:

Takeo Hyodo, Dr.

Graduate School of Science and Technology, Nagasaki University

1-14 Bunkyo-machi, Nagasaki 852-8521, Japan

Tel: +81-95-819-2644

Fax: +81-95-819-2643

E-mail: hyodo@nagasaki-u.ac.jp

Abstract

NO₂-sensing properties of typical oxide (SnO₂, In₂O₃, or WO₃)-based semiconductor gas sensors were measured at 30°C with and without UV-light irradiation (main wavelength: 365 nm), and effects of noble-metal (Pd or Pt) loading, UV-light intensity (0–134 mW cm⁻²) and relative humidity in target gas (0–80%RH) on their NO₂-sensing properties were investigated in this study. The UV-light irradiation effectively reduced the resistances of all sensors, enhanced their NO₂ responses in some cases, and tended to accelerate their response and recovery speeds in dry air, because the UV-light irradiation promoted the adsorption and desorption of NO₂-species on the surface. The SnO₂ sensor showed the largest NO₂ response in dry air, among all the pristine oxide sensors, especially under weak UV-light irradiation (≤ 35 mW cm⁻²), together with relatively fast response and recovery speeds. The Pd or Pt loading onto SnO₂ enhanced the NO₂ response of the SnO₂ sensor and accelerated their response and recovery speeds in dry air, while XPS analysis indicated that most of the Pd and Pt nanoparticles loaded on the surface were oxidized after heat treatment at 500°C. Among all the sensors, the 0.05 wt% Pd-loaded SnO₂ sensor showed the largest NO₂ response under weak UV-light irradiation (≤ 35 mW cm⁻²), together with relatively fast response and recovery speeds. The addition of moisture to the target gas had adverse effects on the NO₂ responses and the response speeds of the SnO₂ and 0.05 wt% Pd-loaded SnO₂ sensors, but the weak UV-light irradiation (7 mW cm⁻²) largely reduced the dependence of the NO₂ response of the 0.05Pd/SnO₂ sensor on relative humidity while maintaining the large NO₂ response, probably because the weak UV-light irradiation promotes the desorption of physisorbed water molecules and then the effective adsorption of NO₂ on the 0.05Pd/SnO₂ surface.

Keywords: NO₂ sensor; UV-light irradiation; tin dioxide; noble metal; room temperature

1. Introduction

Nitrogen dioxides (NO_2), one of gaseous air pollutants in modern society, are emitted in large amounts from various fossil-fuel combustion systems operated at elevated temperatures. Not only does NO_2 cause negative impacts on human health (e.g., an increase in respiratory symptoms and a reduction in pulmonary function) directly [1, 2], but also it reacts with water-based chemicals in the atmosphere to form acid rain causing severe environmental destruction [3]. In addition, NO_2 reacts also with various chemicals (e.g., volatile organic compounds) in the atmosphere under sunlight irradiation, to form other air pollutants such as suspended particulate matters and photochemical oxidants such as ozone, aldehydes, and peroxyacetyl nitrates, and these products also gave a serious risk to human health [4, 5]. Therefore, numerous efforts have been so far directed to developing various types of NO_2 -sensing devices such as solid electrochemical [6–8], optical [9, 10], and acoustic sensors [11, 12]. Among them, it is well known that semiconductor gas sensors show relatively large sensitivity and excellent selectivity to NO_2 at elevated temperatures, and SnO_2 [13–16], In_2O_3 [17–19], WO_3 [20–23], and the related materials are especially promising candidates as the NO_2 -sensing materials, among all the oxide semiconductors. However, the operation of these semiconductor gas sensors at elevated temperatures causes sintering among oxide particles and the grain growth involved, leading to reduction in the NO_2 sensitivity. The UV and/or visible-light irradiation to the semiconductor gas sensors is one of attractive approaches to solving such problems, because it can reduce the sensor resistance to allow the semiconductor gas sensors to operate even at room temperature (RT). Therefore, NO_2 -sensing properties of the semiconductor gas sensors (e.g., SnO_2 [24–26], In_2O_3 [27, 28], WO_3 [29]) under UV and/or visible-light irradiation have been recently reported by many researchers, to improve the disadvantages of the operation at elevated temperatures. We also have already demonstrated that UV-light irradiation (main wavelength: 365 nm) enhanced NO_2 -sensing properties of SnO_2 -based sensors at RT and the

Pd loading onto SnO₂ which was prepared by a hydrothermal method improved their NO₂-sensing properties at RT under UV-light irradiation [30–32]. In this study, differences in NO₂-sensing properties between SnO₂, In₂O₃, and WO₃ sensors with and without UV-light irradiation and effects of the UV-light intensity on their NO₂-sensing properties were first examined at 30°C in air. In addition, impacts of the amount of Pd or Pt loading mainly onto the SnO₂ surface and the amount of moisture (i.e., humidity) in target gas on their NO₂-sensing properties were systematically investigated at 30°C in air.

2. Experimental

2.1 Preparation of SnO₂, In₂O₃, and WO₃ powders and loading of Pd or Pt onto their oxide surface

SnO₂ powder was prepared according to the following procedure. An appropriate amount of NH₄HCO₃ aqueous solution (1.0 mol dm⁻³) was added into SnCl₄ aqueous solution (1.0 mol dm⁻³). The obtained white precipitate was repeatedly centrifuged at a speed of 4500 rpm for 20 min and washed with pure water, and then dried at 100°C for 18 h in ambient air. The resultant powder was calcined at 600°C for 1 h in ambient air, to obtain SnO₂ powder. It was confirmed that the crystal structure of the prepared powder was tetragonal SnO₂ (JCPDS No. 41–1445) by X-ray diffraction (XRD) analysis (Rigaku Corp., RINT2200) using Cu K α radiation (40 kV, 36 mA). In₂O₃ powder, of which crystal structure was assigned to cubic (JCPDS No. 6–416) by XRD analysis, was prepared by pyrolyzing In(NO₃)₃, which was dissolved in pure water, and followed by calcination at 600°C for 1 h in ambient air. WO₃ powder was prepared according to the following procedure. An appropriate amount of HNO₃ aqueous solution (0.8 mol dm⁻³) was added into NaWO₄ aqueous solution (0.15 mol dm⁻³). The yellow resultant precipitate was repeatedly centrifuged at a speed of 4500 rpm for 20 min and washed with pure water, and then dried at 100°C for 18 h in ambient air. The resultant powder was calcined at 500°C for 2 h in

ambient air, to obtain WO_3 powder. It was confirmed that the crystal structure of the prepared powder was monoclinic WO_3 (JCPDS No. 43–1035) by XRD analysis. Specific surface area of the SnO_2 , In_2O_3 , or WO_3 powder obtained, which was measured by the Brunauer–Emmett–Teller (BET) method using N_2 adsorption-desorption isotherms (Micromeritics Instrument Corp., Tristar3000), was 21.2, 23.7, or $12.0 \text{ m}^2 \text{ g}^{-1}$, respectively.

In some cases, Pd or Pt nanoparticles were loaded onto the surface of these oxide powders. After an appropriate amount of oxide powders was added into $\text{Pd}(\text{NO}_3)_2$ or PtCl_4 aqueous solution (0.75 mol dm^{-3}) and then they were ultrasonicated at RT for 1 h, they were evaporated to dryness at 100°C for 2 h in air. The resultant solids were heat-treated at 200°C for 2 h in H_2 to obtain metallic nanoparticles on the oxide surface. The obtained oxide powders loaded with noble metal (N) were denoted as $n\text{N}/\text{MO}$ [n : amount of noble metal (N: Pd or Pt), 0.03–0.10 (wt%)]. Specific surface area of the $n\text{N}/\text{MO}$ powders obtained was hardly influenced by the loading of the noble-metal nanoparticles (e.g., specific surface area of $0.05\text{Pd}/\text{SnO}_2$ powder: ca. $21.0 \text{ m}^2 \text{ g}^{-1}$), because the amount of noble-metal loading onto the oxide surface was really small ($\leq 0.10 \text{ wt}\%$).

Chemical states of the noble metal (Pd or Pt) on the surface of representative $n\text{N}/\text{MO}$ powders were characterized by X-ray photoelectron spectroscopy using Mg $\text{K}\alpha$ radiation (XPS, Kratos, ACIS-TL-TRA DLD), and the binding energy was calibrated using the C 1s level (285.0 eV) from usual contamination. Optical properties of representative oxide powders (SnO_2 and $0.05\text{Pd}/\text{SnO}_2$) were investigated by ultraviolet (UV)–visible (Vis) spectrophotometer (JASCO Corp., V-650) with an integrated sphere (JASCO Corp., ISV-722).

2.2 Fabrication of thick film sensors and measurement of their gas-sensing properties

Thick film sensors were fabricated by screen printing employing the paste of each oxide powder on an alumina substrate equipped with a pair of interdigitated Pt electrodes (gap size:

ca. 500 μm), followed by calcination at 500°C for 1 h in ambient air. The top-view photograph of a representative sensor element, 0.05Pd/SnO₂ sensor, is shown in Fig. 1(a). A thick film sensor was set in a test chamber with a temperature-controlled stage (Lincam Scientific Instr., LST420), which was connected with gas-flow system, and gas responses of these sensors were measured to 5 ppm NO₂ balanced with dry or wet (relative humidity (RH): 20–80%) air at 30°C at a flow rate of 100 cm³ min⁻¹ under UV-light irradiation by using light-emitting diode (UV-LED, Asahi Spectra Co., Ltd., POT-365, main wavelength: 365 nm, irradiation intensity: 0.8–134 mW cm⁻²), after pre-heat treatment at 200°C for several tens of minutes in dry or wet air. The experimental setup for gas-sensing measurements under UV-light irradiation is shown in Fig. 1(b). The magnitude of response to NO₂ was defined as the ratio (R_{NO_2}/R_a) of sensor resistance in NO₂ balanced with air (R_{NO_2}) to that in air (R_a). The $l\%$ response time ($T_{\text{RS}}(l)$) were defined as a period necessary to reach $l\%$ value of the resistance change ($\log R_{\text{NO}_2} - \log R_a$) from the logarithm of sensor resistance in a base gas ($\log R_a$) to that that in NO₂ balanced with air ($\log R_{\text{NO}_2}$, generally after 15 min from the injection of NO₂ in air). The $m\%$ recovery time ($T_{\text{RC}}(m)$) were defined as a period necessary to reach $(100 - m)\%$ value of the resistance change ($\log R_{\text{NO}_2} - \log R_a$) after the injection of NO₂ in air was stopped. The response and recovery times contain a delay period from the gas-switching time to the response- and recovery-starting times, ca. 1.2 min, in this study, since the dead volume of the gas-flow pathway and the chamber in the measurement apparatus is ca. 106 cm³.

3. Results and Discussion

3.1 NO₂-sensing properties of unloaded oxide sensors under UV-light irradiation

Figure 2 shows response transients of a SnO₂ sensor to 5 ppm NO₂ in dry air at 30°C under different UV-light irradiation intensities. Response transients of In₂O₃ and WO₃ sensors to 5 ppm NO₂ in dry air at 30°C under different UV-light irradiation intensities were also shown in

Fig. S1, and variations in their responses (R_{NO_2}/R_a) to 5 ppm NO_2 , resistances in dry air (R_a), and 90% response and 10% recovery times ($T_{\text{RS}}(90)$ and $T_{\text{RC}}(10)$, respectively) with UV-light intensity were summarized in Fig. 3. In addition, typical sensing characteristics of these sensors were shown in Table 1. The resistance of the SnO_2 sensor under no UV-light irradiation was relatively large in dry air (R_a : ca. $2.5 \times 10^5 \Omega$), since SnO_2 was a typical n-type semiconducting oxide and the density of electron carriers was relatively low at 30°C [13–15, 24, 25, 30–32]. In addition, the SnO_2 sensor showed a large positive NO_2 response (ca. 81) under no UV-light irradiation. The behavior indicates that a large amount of NO_2 molecules negatively chemisorbed as NO_2^- on the SnO_2 surface, trapping electron from the SnO_2 bulk [13–15]. However, the response speed was really slow ($T_{\text{RS}}(90)$: ca. 12 min) and the sensor showed little recovery behavior ($T_{\text{RC}}(10)$: ca. 30 min). Weak UV-light irradiation abruptly decreased the resistance of the SnO_2 sensor in dry air (e.g., R_a : ca. $1.2 \times 10^4 \Omega$ at 7 mW cm^{-2}) and the further increase in the UV-light intensity decreased the resistance gradually, because the UV-light irradiation excited electrons in the SnO_2 bulk to the conduction band and/or it reduced negatively oxygen adsorbates (mainly, O_2^-) on the SnO_2 surface [25, 33]. The NO_2 response of the SnO_2 sensor under weak UV-light irradiation (especially, $\leq 7 \text{ mW cm}^{-2}$) was much larger than that under no UV-light irradiation, but the further increase in the UV-light intensity (more than 35 mW cm^{-2}) decreased the NO_2 response, in comparison with that under no UV-light irradiation. The response speed was hardly improved by the weakest UV-light irradiation (0.8 mW cm^{-2}). The further increase in the UV-light intensity ($\geq 7 \text{ mW cm}^{-2}$) was quite effective in reducing the response time, but the response time was less dependent on the UV-light intensity in the range between 7 mW cm^{-2} and 134 mW cm^{-2} . On the other hand, the recovery speed was relatively improved even by the weakest UV-light irradiation ($T_{\text{RC}}(10)$: ca. 5.1 min at 0.8 mW cm^{-2}), and the further increase in UV-light intensity tended to reduce the recovery time, probably because the UV-light irradiation promoted the desorption of NO_2^- on the SnO_2 surface.

However, even strong UV-light irradiation was not able to turn the resistance in dry air back to the original level before the NO₂ injection, during the measurement period. These facts indicate that the injection of photon energy into the SnO₂ was effective in enhancing chemical adsorption/desorption of NO₂ on the SnO₂ surface and the balance between adsorption and desorption of NO₂ probably determined not only the magnitude of NO₂ response but also the response and recovery speeds.

The effects of UV-light irradiation on the NO₂-sensing properties of In₂O₃ and WO₃ sensors are fundamentally similar to those of the SnO₂ sensor, but some important behavior was different among them. The resistance of both the sensors decreased with an increase in UV-light intensity, as is the case with that of the SnO₂ sensor. The resistance of the In₂O₃ sensor was smaller than that of the SnO₂ sensor, while the resistance of the WO₃ sensor was larger than that of the SnO₂ sensor, with or without UV-light irradiation. The In₂O₃ sensor showed the largest NO₂ response among all the pristine oxide sensors when UV light was not irradiated. However, even weak UV-light irradiation largely reduced the NO₂ response of the In₂O₃ sensor and the NO₂ response decreased with an increase in UV-light intensity. Thus, the NO₂ response of the In₂O₃ sensor under UV-light irradiation was much smaller than that of the SnO₂ sensor. The dependence of response and recovery speeds of the In₂O₃ sensor on UV-light intensity was also quite similar to those of the SnO₂ sensor, and the UV-light irradiation was effective in reducing the response and recovery times. On the other hand, the NO₂ response of the WO₃ sensor was not able to be confirmed under no UV-light irradiation, because the resistance in 5 ppm NO₂ balanced with dry air was too high to be measured with the measurement apparatus used in this study. However, the magnitude of NO₂ response of the WO₃ sensor under no UV-light irradiation was over 900, which was larger than that of the SnO₂ sensor. The large NO₂ response of the WO₃ sensor under no UV-light irradiation in comparison with other oxide sensors has already been reported by several researchers [19–22]. The UV-light irradiation drastically

reduced the NO₂ response, and the NO₂ response of the WO₃ sensor under UV-light irradiation was the smallest among all the sensors under all the UV-light irradiation range. The response and recovery speeds under no UV-light irradiation were not also be calculated because of too high resistance in 5 ppm NO₂ balanced with dry air beyond the range of measurement, and thus the effect of the UV-light irradiation on the response and recovery speeds was not able to be discussed in this study. However, the response and recovery speeds of the WO₃ sensor even under UV-light irradiation were much slower than those of the SnO₂ and In₂O₃ sensors. These results indicate that the WO₃ sensor, which generally shows large NO₂ response at elevated temperatures, is not suitable for detecting NO₂ at RT under UV-light irradiation. Considering the above results based on the impacts of the UV-light intensity on the magnitude of their NO₂ responses, we should investigate the NO₂-sensing properties of these sensors under much weaker UV-light irradiation, but such weak UV-light irradiation ($< 0.8 \text{ mW cm}^{-2}$) is out of control for our experimental setup. In addition, the too slow response and recovery speeds of the WO₃ sensor under weak UV-light irradiation presently make our interests go away from the investigation in this study, especially from the aspect of the practice use. As mentioned above, the WO₃ sensor as well as the In₂O₃ sensor showed smaller NO₂ responses under UV-light irradiation at ca. 365 nm in this study, than that of the SnO₂ sensor. However, the In₂O₃ and WO₃ sensors may be able to detect NO₂ and other gases more sensitively under visible-light irradiation in comparison with the SnO₂ sensor, because the band gaps of In₂O₃ [28] and WO₃ [29] were generally lower than that of SnO₂. The impacts of wavelength of irradiated light on the gas-sensing properties of these sensors will be investigated in the near future.

3.2 Effects of Pd loading onto SnO₂ and In₂O₃ sensors on their NO₂-sensing properties

Effects of Pd loading onto both the SnO₂ and In₂O₃ sensors, which showed much excellent NO₂-sensing properties and relatively lower resistance in dry air under UV-light irradiation than

the WO_3 sensor, on the NO_2 -sensing properties were investigated in this study. Figure 4 shows response transients of representative $n\text{Pd}/\text{SnO}_2$ sensors (n : 0.05 and 0.07) to 5 ppm NO_2 at 30°C in dry air under different UV-light irradiation intensities. In addition, Fig. 5 shows variations in response to 5 ppm NO_2 and resistance of all $n\text{Pd}/\text{SnO}_2$ sensors in dry air with the amount of Pd loaded, and Fig. S2 shows variations in 90% response and 60% recovery times of all $n\text{Pd}/\text{SnO}_2$ sensors with UV-light intensity, together with those of the SnO_2 sensor. Typical sensing characteristics of the $0.05\text{Pd}/\text{SnO}_2$ sensor were shown also in Table 1. Here, the resistance of most of $n\text{Pd}/\text{SnO}_2$ sensors under no UV-light irradiation was instable in 5 ppm NO_2 balanced with dry air, and the NO_2 -sensing property of only the $0.05\text{Pd}/\text{SnO}_2$ sensor was able to be measured under no UV-light irradiation. The Pd loading onto the SnO_2 surface increased the resistance in dry air with or without UV-light irradiation. It is well known that Pd nanoparticles are oxidized by heat treatment at elevated temperatures in air [34–36]. Therefore, XPS spectra of Pd on the surface of representative $n\text{Pd}/\text{SnO}_2$ powders (n : 0.05 and 0.10) after the heat treatment at 500°C for 1 h in ambient air, which is the same heat-treatment condition as the sensor fabrication, were investigated as shown in Fig. 6. The obtained XPS spectra of Pd $3d_{5/2}$ and $3d_{3/2}$ obviously exhibited that the heat treatment at 500°C oxidized almost all Pd nanoparticles on the surface of $0.05\text{Pd}/\text{SnO}_2$ and $0.10\text{Pd}/\text{SnO}_2$ powders, to form PdO [36]. The electron affinity of PdO (ca. 5.5 eV) [34] are larger than that of SnO_2 (ca. 4.5 eV) [37, 38], and therefore electrons of SnO_2 are likely transferred into the PdO nanoparticles. This is the reason why the resistance of $n\text{Pd}/\text{SnO}_2$ sensors in dry air increased with an increase in the amount of Pd loading, as shown in Fig. 5(b). In addition, the resistance of all the $n\text{Pd}/\text{SnO}_2$ sensors monotonically decreased with an increase in UV-light intensity, as is the case with the SnO_2 sensor. The Pd loading effectively enhanced the NO_2 response of the SnO_2 sensor, probably because the large amount of NO_2 molecules directly adsorbed on the surface of PdO nanoparticles and SnO_2 and/or the NO_2 species adsorbed on the PdO surface spilt over onto the

SnO₂ surface. The UV-light irradiation drastically changed their response behavior to 5 ppm NO₂ at 30°C in dry air. Namely, all the *n*Pd/SnO₂ sensors showed the largest NO₂ response under UV-light irradiation of 7 mW cm⁻² (ca. 3.4×10³ for 0.05Pd/SnO₂), their NO₂ responses decreased with an increase in the UV-light intensity, regardless of the amount of Pd loaded onto the SnO₂ surface, and thus the NO₂ responses of SnO₂ and 0.05Pd/SnO₂ sensors under strong UV-light irradiation of 75 and 134 mW cm⁻² was lower than those under no UV-light irradiation. Then, the 0.05Pd/SnO₂ sensor showed the largest NO₂ response among all the sensors at every UV-light intensity. The 0.05Pd/SnO₂ sensor, which only had relatively stable NO₂ response among all the *n*Pd/SnO₂ sensors under no UV-light irradiation, showed quite slow response speed without recovery behavior under no UV-light irradiation, as is the case with the SnO₂ sensor. The weak UV-light irradiation stabilized the NO₂-response behavior of the *n*Pd/SnO₂ sensors and drastically accelerated the response speeds of all the *n*Pd/SnO₂ sensors to NO₂ (e.g., $T_{RS}(90)$: ca. 2.8 min for the 0.05Pd/SnO₂ sensor at 7 mW cm⁻²), but the further increase in UV-light irradiation tended to slow down the response speeds (e.g., $T_{RS}(90)$: ca. 6.7 min for the 0.05Pd/SnO₂ sensor at 134 mW cm⁻²). On the other hand, an increase in UV-light irradiation tended to improve the recovery speeds of all the *n*Pd/SnO₂ sensors to NO₂ (e.g., $T_{RC}(60)$: ca. 5.5 min, for the 0.05Pd/SnO₂ sensor at 134 mW cm⁻²).

The resistance change of SnO₂ and 0.05Pd/SnO₂ sensors with O₂ injection into dry N₂ was investigated at 30°C with and without UV-light irradiation, to clarify the effects of adsorption and desorption of oxygen species on their resistances. Figure 7 shows representative response transients of the SnO₂ and 0.05Pd/SnO₂ sensors to 30% O₂ in dry N₂ at 30°C and variations in response of these sensors to 30% O₂ in dry N₂ at 30°C with UV-light intensity. The magnitude of response to 30% O₂ in dry N₂ was defined as the ratio of sensor resistance in 30% O₂ balanced with dry N₂ (after 70 min upon exposure to O₂) to that in dry N₂. These sensors were heat-treated in dry N₂ at 200°C for 2 h, prior to the measurement, to remove oxygen species (O₂⁻)

which are adsorbed on the SnO₂ surface. The resistance of the SnO₂ sensor was smaller than that of the 0.05Pd/SnO₂ sensor even in dry N₂ with or without UV-light irradiation, and the UV-light irradiation reduced these resistances in dry N₂, as is the cases in dry air. These facts under the O₂-free atmosphere strongly supports that electrons in SnO₂ and 0.05Pd/SnO₂ bulk excited from valence band and/or some defect levels to the conduction band by the UV-light irradiation, because most of oxygen species (O₂⁻) on their surface should be desorbed by the pre-heat treatment in N₂ at 200°C. Figure 8 shows diffuse reflectance UV–Vis spectra (normalized Kubelka–Munk function $(F(r)/F(r)_{MAX})$ vs. wavelength, where r stands for reflectance and $F(r)_{MAX}$ is the maximum of Kubelka–Munk function ($F(r)$) of SnO₂ and 0.05Pd/SnO₂ powders, together with their Tarc plots ($(hvF(r))^2$ vs. photon energy, where h and ν stand for Plank constant and frequency, respectively [39]). Band gaps (E_g) of SnO₂ and 0.05Pd/SnO₂, which was determined from the Tarc plots, were ca. 3.5 eV and ca. 3.7 eV, respectively, which were closely correspondent with those of typical SnO₂, 3.4–3.8 eV [38, 40, 41]. The difference in E_g between SnO₂ and 0.05Pd/SnO₂ probably depends on whether or not PdO nanoparticles were loaded onto their surfaces and/or they were heat-treated at 200°C under H₂ atmosphere. Since the band-gap energies of SnO₂ and 0.05Pd/SnO₂ powders are slightly larger than main photon energy of UV light emitted from the UV-LED (ca. 3.40 eV, which was calculated from the main wavelength, 365 nm), electrons in valence band cannot easily excite to the conduction band. However, the optical absorption edge up to the range of visible light (i.e., >400 nm) was observed for the SnO₂ and 0.05Pd/SnO₂ powders, which are pale yellow and pale brown, respectively, in Fig. 8. The absorption probably arises from some energy levels of various defects such as oxygen vacancies [40], since these powders were prepared under relatively moderate condition (at 600°C for 1 h in ambient air). These optical properties are one of the reasons why the UV-light irradiation reduced even the resistance of both the sensors in dry N₂ (see Fig. 7). The injection of 30% O₂ in dry N₂ increased the resistance of both the sensors with

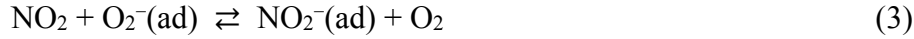
or without UV-light irradiation, because oxygen species negatively adsorbed on the oxide surface, according to the forward reaction of the following equation [25, 33].



However, the resistances of both the sensors even after 70 min upon exposure to 30% O₂ in dry N₂ (ca. $1.2 \times 10^3 \ \Omega$ and ca. $3.0 \times 10^4 \ \Omega$ for SnO₂ and 0.05Pd/SnO₂ sensors, respectively) were much smaller than those in dry air (21% O₂) (ca. $2.3 \times 10^5 \ \Omega$ and ca. $4.0 \times 10^5 \ \Omega$ for SnO₂ and 0.05Pd/SnO₂ sensors, respectively, cf. Figs. 2–5) under no UV-light irradiation. On the other hand, the UV-light irradiation improved the rate of resistance change of both the sensors. Namely, the resistance of the SnO₂ sensor after 70 min upon exposure to 30% O₂ in dry N₂ under UV-light irradiation (e.g., ca. $7.9 \times 10^2 \ \Omega$ at $134 \ \text{mW cm}^{-2}$) was slightly smaller than those in dry air (21% O₂) (e.g., ca. $3.2 \times 10^3 \ \Omega$ at $134 \ \text{mW cm}^{-2}$) and the resistance of the 0.05Pd/SnO₂ sensor after 70 min upon exposure to 30% O₂ in dry N₂ under UV-light irradiation (e.g., ca. $4.5 \times 10^3 \ \Omega$ at $134 \ \text{mW cm}^{-2}$) was already larger than those in dry air (21% O₂) (e.g., ca. $4.0 \times 10^3 \ \Omega$ at $134 \ \text{mW cm}^{-2}$). These results obviously show that the UV-light irradiation enhanced the rate of the forward reaction of the eq. (1), producing the large amount of negatively adsorbed oxygen species (O₂⁻). In addition, the behavioral difference between these sensors indicates that PdO nanoparticles on the SnO₂ surface accelerated the adsorption of O₂⁻ onto the surface and the adsorption rate of oxygen species on the PdO surface (and/or the amounts) was larger than that on the SnO₂ surface. Furthermore, the UV-light irradiation drastically accelerated also the desorption rate of negatively adsorbed oxygen species (i.e., the reverse reaction of eq. (1)), on the basis that the resistances of both the sensors smoothly decreased after the injection of O₂ in dry N₂ was stopped. However, large NO₂ responses of the SnO₂ and 0.05Pd/SnO₂ sensors with their fast response speed and slow recovery speed in dry air (see Figs. 2–4 and S2) shows that NO₂ molecules promptly adsorbed even onto the oxide surface which was covered with O₂⁻ adsorbed, according to the forward reaction of the following equation [24, 42].



In summary, the forward reaction of the following equation promptly proceeds even in a low concentration (5 ppm) of NO₂ balanced with dry air (21% O₂), probably because the adsorption energy of NO₂ onto the surface (eq. (2)) is much larger than that of O₂ (eq. (1)).



In addition, Ruhland et al. reported that physisorbed NO₂ molecules form deeper acceptor levels on the SnO₂ surface than negatively adsorbed oxygen species (O₂⁻), and thus bound electrons are transferred from the O₂⁻ to physisorbed NO₂ molecules forming NO₂⁻ species [43]. The deep acceptor levels which are formed by NO₂⁻ species on the oxide surface is the main reason of large resistances of the sensors in NO₂ balanced with dry air. Furthermore, Fig. 7 shows the response of the 0.05Pd/SnO₂ sensor to 30% O₂ was larger than that of the SnO₂ sensor in dry N₂ and the recovery speed of the 0.05Pd/SnO₂ sensor was faster than that of the SnO₂ sensor. This is probably because PdO nanoparticles on the SnO₂ surface accelerated the adsorption and desorption of O₂, which is one of important factors in determining faster response and recovery speeds of the 0.05Pd/SnO₂ sensor to NO₂ than that of the SnO₂ sensor.

On the other hand, an increase in UV-light intensity reduced the magnitude of NO₂ response of these sensors. It is well known that NO₂ was converted to NO and atomic oxygen under UV-light irradiation, according to the following reaction [44].



In addition, an increase in UV-light intensity reduces the amount of adsorbed NO₂⁻ on the oxide surface, and thus accelerates the reverse reaction of eq. (2). It is expected that these reactions were promoted with increasing UV-light intensity to decrease the NO₂ response of these sensors. Furthermore, an increase in UV-light intensity improved the response and recovery speeds of both the sensors, because the rates of adsorption and desorption of O₂ and NO₂ increased with increasing UV-light intensity.

Figure S3 shows response transients of $0.05\text{Pd}/\text{In}_2\text{O}_3$ and $0.07\text{Pd}/\text{In}_2\text{O}_3$ sensors to 5 ppm NO_2 at 30°C in dry air under different UV-light irradiation intensities, and Fig. S4 shows variations in response of these sensors to 5 ppm NO_2 and resistance in dry air with the amount of Pd loaded and UV-light intensity, respectively. In addition, an XPS spectrum of Pd $3d_{5/2}$ and $3d_{3/2}$ on the surface of representative $n\text{Pd}/\text{In}_2\text{O}_3$ powder ($n: 0.07$) after heat treatment at 500°C for 1 h in ambient air is shown in Fig. S5. The XPS spectrum of Pd was quite similar to those of $0.05\text{Pd}/\text{SnO}_2$ and $0.10\text{Pd}/\text{SnO}_2$ powders (Fig. 6), which indicates that most of the Pd nanoparticles loaded on the $0.07\text{Pd}/\text{In}_2\text{O}_3$ powder were also oxidized to form PdO [36]. The resistance in dry air increased with an increase in the amount of Pd loaded onto In_2O_3 , because of smaller electron affinity of In_2O_3 (ca. 3.7 eV) [45] than the electron affinity of PdO, and it decreased with an increase in UV-light intensity, as is the case with the $n\text{Pd}/\text{SnO}_2$ sensors. However, even the response of the $0.05\text{Pd}/\text{In}_2\text{O}_3$ sensor to 5 ppm NO_2 under UV-light irradiation of 7 mW cm^{-2} (ca. 38), which was the largest among those of the $n\text{Pd}/\text{In}_2\text{O}_3$ sensors, was much smaller than that of the $0.05\text{Pd}/\text{SnO}_2$ sensor (R_{NO_2}/R_a : ca. 3.4×10^3). The response times of the $n\text{Pd}/\text{In}_2\text{O}_3$ sensors (e.g., $T_{\text{RS}}(90)$: ca. 3.2 min and ca. 3.0 min for the $0.05\text{Pd}/\text{In}_2\text{O}_3$ sensor at 7 and 134 mW cm^{-2} , respectively) were comparable to (or faster than, in some cases) those of the $n\text{Pd}/\text{SnO}_2$ sensors (e.g., $T_{\text{RS}}(90)$: ca. 2.8 min and ca. 6.8 min for the $0.05\text{Pd}/\text{SnO}_2$ sensor at 7 and 134 mW cm^{-2} , respectively), while the recovery times of the $n\text{Pd}/\text{In}_2\text{O}_3$ sensors (e.g., $T_{\text{RC}}(60)$: ca. 37 min and ca. 30 min for the $0.05\text{Pd}/\text{In}_2\text{O}_3$ and $0.07\text{Pd}/\text{In}_2\text{O}_3$ sensors at 7 mW cm^{-2} , respectively) were much longer to those of the $n\text{Pd}/\text{SnO}_2$ sensors (e.g., $T_{\text{RC}}(60)$: ca. 16 min and ca. 17 min for the $0.05\text{Pd}/\text{SnO}_2$ and $0.07\text{Pd}/\text{SnO}_2$ sensors at 7 mW cm^{-2} , respectively). These results show that the Pd loading was not effective in improving the NO_2 -sensing properties of the In_2O_3 sensor under UV-light irradiation at least, in comparison with those of the SnO_2 sensor. Hereafter, the gas-sensing properties of the $n\text{Pd}/\text{In}_2\text{O}_3$ sensors should be measured under visible-light irradiation, together with those of both the In_2O_3 and WO_3

sensors as shown in Section 3.1, to clarify the potential as a light-driven gas sensor which can be operated in the vicinity of room temperature.

3.3 Effects of Pt loading onto SnO₂ sensor on the NO₂-sensing properties

Effects of Pt loading on the NO₂-sensing properties of the SnO₂ sensor were also investigated in this study. XPS spectra of Pt 4f_{7/2} and 4f_{5/2} on the surface of prepared *n*Pt/SnO₂ powders (*n*: 0.05 and 0.10) after heat treatment at 500°C for 1 h in ambient air, which is the same heat-treatment condition as the sensor fabrication, are shown in Fig. 9. A major majority of the Pt nanoparticles loaded on both the powders (~90%) was oxidized after the heat treatment, to turn into PtO₂ and PtO (Pt⁴⁺:Pt²⁺:Pt (metal) = 50.9:38.6:10.5 for 0.05Pt/SnO₂ and 57.5:33.3:9.2 for 0.10Pt/SnO₂) [46]. Figure S6 shows response transients of 0.05Pt/SnO₂ and 0.10Pt/SnO₂ sensors to 5 ppm NO₂ at 30°C in dry air under UV-light irradiation, and Fig. 10 shows variations in response of these sensors to 5 ppm NO₂ with UV-light intensity, together with those of the SnO₂, 0.05Pd/SnO₂ and 0.10Pd/SnO₂ sensors. In addition, typical sensing characteristics of the 0.05Pt/SnO₂ sensor were shown in Table 1. The resistance of these sensors in dry air, which increased with an increase in the amount of Pt loaded onto SnO₂, also decreased with an increase in UV-light intensity. The 0.05 wt% Pt loading improved the NO₂ response and the response speed of the SnO₂ sensor under every UV-light irradiation intensity (e.g., R_{NO_2}/R_a : ca. 1.5×10^3 and $T_{\text{RS}}(90)$: ca. 3.2 min for the 0.05Pt/SnO₂ sensor at 7 mW cm⁻²), but the effectiveness was smaller than that of the 0.05 wt% Pd loading, especially under higher UV-light irradiation. On the other hand, the 0.05 wt% Pt loading was effective in improving only the recovery speed under every UV-light irradiation intensity (e.g., $T_{\text{RC}}(60)$: ca. 13 and ca. 3.5 min for the 0.05Pt/SnO₂ sensor at 7 and 134 mW cm⁻², respectively). However, an increase in the amount of Pt loading (i.e., 1.0 wt% Pt loading) tended to slow down the response and recovery speeds as well as to reduce the NO₂ response. These results indicate that the Pd loading

onto the SnO₂ surface was more effective in improving the NO₂-sensing properties of the SnO₂ sensor at 30°C in dry air under UV-light irradiation, than the Pt loading.

3.4 Effects of humidity in gaseous atmosphere on the NO₂-sensing properties of SnO₂ and 0.05Pd/SnO₂ sensors

Figure S7 shows representative response transients of SnO₂ and 0.05Pd/SnO₂ sensors to 5 ppm NO₂ in wet air (80%RH), and Fig. 11 shows variations in response (R_{NO_2}/R_a) of these sensors to 5 ppm NO₂ in air at 30°C under different UV-light irradiation intensities with relative humidity. The addition of moisture into air drastically had great impacts on the NO₂-sensing properties of both the sensors. The resistances of both the sensors in wet air (80%RH) decreased with an increase in UV-light intensity, as is the case with those in dry air. The resistance of the SnO₂ sensor in wet air (80%RH) under no UV-light intensity (ca. $2.2 \times 10^5 \Omega$) was slightly smaller than that in dry air (ca. $2.5 \times 10^5 \Omega$, see Figs. 2 and 3), and the addition of moisture did not have a considerable influence on the resistance in air, even under UV-light irradiation. These results imply that adsorbed water molecules have only a little influence on the adsorption state of oxygen adsorbates (O_2^-) on the SnO₂ surface. The loading of 0.05 wt% Pd largely increased the resistance of the SnO₂ sensor, also in wet air (80%RH) and the addition of moisture into air largely decreased the resistance of the 0.05Pd/SnO₂ sensor, with or without UV irradiation (e.g., ca. $6.3 \times 10^5 \Omega$ in dry air (see Figs. 4 and 5) and ca. $2.8 \times 10^5 \Omega$ in wet air (80%RH) under no UV irradiation, and ca. $2.5 \times 10^4 \Omega$ in dry air (see Figs. 4 and 5) and ca. $2.5 \times 10^3 \Omega$ in wet air (80%RH) under UV irradiation at 75 mW cm^{-2}). These facts indicate that the loaded PdO nanoparticles enhanced the adsorption of water molecules on the SnO₂ surface and then the adsorbed water molecules reduced the resistance of the 0.05Pd/SnO₂ sensor at 30°C [31]. These effects of the Pd loading on the resistance of a SnO₂ sensor at 30°C under UV-light irradiation seem to be different from those at elevated temperatures [47]. The injection of NO₂ in wet air

increased the resistance of both the sensors with or without UV-light irradiation, but the impacts of the moisture addition on the NO₂-response behavior were dependent on the relative humidity and the UV-light intensity. The NO₂ response of the SnO₂ sensor drastically decreased with an increase in the relative humidity under no UV-light irradiation, and the SnO₂ sensor showed only a small NO₂ response (R_{NO_2}/R_a at 80%RH: ca. 1.4) in air containing a large amount of moisture under no UV-light irradiation. The UV-light irradiation enhanced the NO₂ response of the SnO₂ sensor in wet air, and the NO₂ response of the SnO₂ sensor in wet air under UV-light irradiation tended to increase with a decrease in UV-light intensity. However, the NO₂ responses of the SnO₂ sensor in wet air ($\geq 40\%$ RH) even under weak UV-light irradiation (7 and 35 mW cm⁻²) were much smaller than those in dry air (see Figs. 2 and 3). On the other hand, the further increase in UV-light intensity (namely, at 75 and 134 mW cm⁻²) seems to decrease the dependency of relative humidity on the NO₂ response of the SnO₂ sensor, probably because the UV-light irradiation reduced the adsorption of water molecules on the SnO₂ surface. The addition of moisture in air also led to slow down the response speed under UV-light irradiation (especially at 7 mW cm⁻², $T_{\text{RES}}(90)$: ca. 27.5 min in wet air (80%RH) in comparison with ca. 4.6 min in dry air (see Figs. 2 and 3)). These NO₂-sensing properties of the SnO₂ sensor show that a large amount of physisorbed water molecules, which do not contribute to a reduction in the sensor resistance, exist on the SnO₂ surface in wet air with or without UV-light irradiation and they interfered the negatively charged adsorption of NO₂ onto the SnO₂ surface. However, the injection of a large amount of photon energy to the SnO₂ sensor (i.e., strong UV-light irradiation at 75 and 134 mW cm⁻²) is likely to promote the desorption of the physisorbed water molecules on the SnO₂ surface in wet air, to reduce the RH dependence of the NO₂ response.

On the other hand, the injection of NO₂ unstabilized the resistance of the 0.05Pd/SnO₂ sensor in wet air (80%RH) under no UV-light irradiation even though the resistance in wet air (80%RH) was able to be somehow measured (R_a at 80%RH: ca. $2.5 \times 10^5 \Omega$), and thus the

response transient of the $0.05\text{Pd}/\text{SnO}_2$ sensor in wet air (80%RH) under no UV-light irradiation is not shown in Figs. S7 and 11. The NO_2 response of the $0.05\text{Pd}/\text{SnO}_2$ sensor was much larger than that of the SnO_2 sensor, also in wet air under each UV-light irradiation intensity, and the NO_2 response also tended to decrease with an increase in the relative humidity and UV-light intensity. In addition, the NO_2 response at stronger UV-light irradiation ($\geq 35 \text{ mW cm}^{-2}$) was largely dependent on the relative humidity (especially in the range of 0–40%RH (a small amount of relative humidity)). The stronger UV-light irradiation probably promoted the production of hydroxyl groups from physisorbed water molecules on the $0.05\text{Pd}/\text{SnO}_2$ surface, to inhibit the adsorption of NO_2 . On the other hand, the NO_2 response under the weakest UV-light irradiation (namely, at 7 mW cm^{-2}) was the largest among all conditions, and it showed the smallest dependency of the NO_2 response of the $0.05\text{Pd}/\text{SnO}_2$ sensor on the relative humidity ($R_{\text{NO}_2}/R_{\text{a}}$: ca. 1.9×10^3 in wet air (80%RH) at 7 mW cm^{-2}). These results probably indicate that a small amount of photon energy (i.e., $\leq 7 \text{ mW cm}^{-2}$) promotes the desorption of physisorbed water molecules and then the effective adsorption of NO_2 on the $0.05\text{Pd}/\text{SnO}_2$ surface. The response speed of the $0.05\text{Pd}/\text{SnO}_2$ sensor in wet air (80%RH) was quite slower than that in dry air. In addition, the $0.05\text{Pd}/\text{SnO}_2$ sensor showed the fastest response speed in wet air (80%RH) under the weakest UV-light irradiation ($T_{\text{RS}}(90)$: ca. 8.4 min at 7 mW cm^{-2}), and the response speed tended to slow down with an increase in UV-light intensity in spite of the small NO_2 response (e.g., $T_{\text{RS}}(90)$: ca. 11.8 min at 134 mW cm^{-2}). On the other hand, the recovery speed of the $0.05\text{Pd}/\text{SnO}_2$ sensor was hardly dependent on relative humidity (e.g., $T_{\text{RC}}(60)$ in wet air (80%RH): ca. 18.9 min and 5.3 min at 7 mW cm^{-2} and 134 mW cm^{-2} , respectively, and $T_{\text{RC}}(60)$ in dry air (cf. Figs. 2 and 3): ca. 16.1 min and 5.5 min at 7 mW cm^{-2} and 134 mW cm^{-2} , respectively), and the recovery speed in wet air also increased with an increase in UV-light intensity, as is the case in dry air. The behavior probably indicates that the desorption rate of NO_2^- accelerated with an increase in UV-light intensity, but physisorbed

water molecules and hydroxyl groups on the $0.05\text{Pd}/\text{SnO}_2$ surface have little influence on the desorption rate of NO_2^- under UV-light irradiation.

Conclusion

Effects of noble-metal loading onto typical semiconducting oxides (SnO_2 , In_2O_3 , and WO_3), intensity of UV-light irradiation to these sensors and addition of moisture in target gas on the NO_2 -sensing properties of the oxides-based semiconductor gas sensors were investigated in air at 30°C in this study. The UV-light irradiation effectively reduced the resistances of all the pristine oxide sensors and accelerated the response and recovery speeds of the SnO_2 and In_2O_3 sensors in dry air, while the magnitude of response of all the sensors to 5 ppm NO_2 tended to decrease with an increase in UV-light intensity. However, only the SnO_2 sensor showed larger NO_2 response in dry air under weak UV-light irradiation ($\leq 35 \text{ mW cm}^{-2}$) than that under no UV-light irradiation. The Pd loading increased the sensor resistance and enhanced the NO_2 response of the SnO_2 sensor in dry air under every UV-light irradiation intensity. In addition, the Pd loading accelerated the response speeds of the SnO_2 sensor mainly under weak UV-light irradiation ($\leq 35 \text{ mW cm}^{-2}$), while the recovery speeds of the $n\text{Pd}/\text{SnO}_2$ sensors were faster than that of the SnO_2 sensors under every UV-light irradiation intensity. The difference in these NO_2 -sensing properties of SnO_2 and $n\text{Pd}/\text{SnO}_2$ sensors in dry air with and without UV-light irradiation seems to arise from adsorption-desorption rates of NO_2 and O_2 on each oxide surface under each UV-light irradiation intensity. In addition, the Pd loading onto the SnO_2 sensor was more effective in improving the NO_2 -sensing properties than the Pt loading onto the SnO_2 sensor as well as the Pd loading onto the In_2O_3 sensor. On the other hand, the addition of moisture in target gas tended to reduce the magnitude of NO_2 responses of both the SnO_2 and $0.05\text{Pd}/\text{SnO}_2$ sensors and slowed down their response speeds, but the $0.05\text{Pd}/\text{SnO}_2$ sensor maintained relatively large NO_2 response and fast response speed even in wet air, only under weak UV-light irradiation (7 mW cm^{-2}).

References

1. D. L. Jarvis, B. P. Leaderer, S. Chinn, P. G. Burney, Indoor nitrous acid and respiratory symptoms and lung function in adults, *Thorax* 60 (2005) 474–479.
2. A. J. Chauhan, S. L. Johnston, Air pollution and infection in respiratory illness, *British Medical Bulletin* 68 (2003) 95–112.
3. D. A. Burns, J. Aherne, D. A. Gay, C. M. B. Lehmann, Acid rain and its environmental effects: Recent scientific advances, *Atmos. Environ.* 146 (2016) 1–4.
4. Y. Kanaya, H. Tanimoto, J. Matsumoto, H. Furutani, S. Hashimoto, Y. Komazaki, S. Tanaka, Y. Yokouchi, S. Kato, Y. Kajii, H. Akimoto, Diurnal variations in H₂O₂, O₃, PAN, HNO₃ and aldehyde concentrations and NO/NO₂ ratios at Rishiri Island, Japan: Potential influence from iodine chemistry, *Sci. Total Environ.* 376 (2007) 185–197.
5. A. Notario, I. Bravo, J. A. Adame, Y. Díaz-de-Mera, A. Aranda, A. Rodríguez, D. Rodríguez, Analysis of NO, NO₂, NO_x, O₃ and oxidant (O_x=O₃+NO₂) levels measured in a metropolitan area in the southwest of Iberian Peninsula, *Atmos. Res.* 104–105 (2012) 217–226.
6. M. Ono, K. Shimano, N. Miura, N. Yamazoe, Solid-state amperometric sensor based on a sodium ion conductor for detection of total NO_x in an atmospheric environment, *Electrochem. Solid State Lett.* 2 (1999) 349–351.
7. J. W. Yoon, M. L. Grilli, E. Di Bartolomeo, R. Polini, E. Traversa, The NO₂ response of solid electrolyte sensors made using nano-sized LaFeO₃ electrode, *Sens. Actuators B* 76 (2001) 483–488.
8. T. Ueda, M. Sakai, K. Kamada, T. Hyodo, Y. Shimizu, Effects of composition and structure of sensing electrode on NO₂ sensing properties of mixed potential-type YSZ-based gas sensors, *Sens. Actuators B* 237 (2016) 247–255.
9. T. Nezel, A. Fakler, G. Zhylyak, G. J. Mohr, U. E. Spichiger-Keller, A highly sensitive NO₂-

- selective optode membrane, *Sens. Actuators B* 70 (2000) 165–169.
10. A. Paliwal, A. Sharma, M. Tomar, V. Gupta, Room temperature detection of NO₂ gas using optical sensor based on surface plasmon resonance technique, *Sens. Actuators B* 216 (2015) 497–503.
 11. M. Penza, L. Vasanelli, SAW NO_x gas sensor using WO₃ thin-film sensitive coating, *Sens. Actuators B* 41 (1997) 31–36.
 12. H. Seh, T. Hyodo, H. L. Tuller, Bulk acoustic wave resonator as a sensing platform for NO_x at high temperatures, *Sens. Actuators B* 108 (2005) 547–552.
 13. G. Sberveglieri, G. Faglia, S. Groppelli, P. Nelli, Methods for the preparation of NO, NO₂ and H₂ sensors based on tin oxide thin films, grown by means of the r.f. magnetron sputtering technique, *Sens. Actuators B* 8 (1995) 388–391.
 14. T. Hyodo, K. Sasahara, Y. Shimizu, M. Egashira, Preparation of macroporous SnO₂ films using PMMA microspheres and their sensing properties to NO_x and H₂, *Sens. Actuators B* 106 (2005) 580–590.
 15. A. A. Firooz, T. Hyodo, A. Reza Mahjoub, A. Ali Khodadadi, Y. Shimizu, Synthesis and Gas-sensing Properties of Nano- and Meso-porous MoO₃-doped SnO₂, *Sens. Actuators B* 147 (2010) 554–560.
 16. H.-Y. Li, Z.-X. Cai, J.-C. Ding, Z. Guo, Gigantically enhanced NO sensing properties of WO₃/SnO₂ double layer sensors with Pd decoration, *Sens. Actuators B* 220 (2015) 398–405.
 17. A. Gurlo, M. Ivanovskaya, N. Bârsan, M. Schweizer-Berberich, U. Weimar, W. Göpel, A. Diéques, Grain size control in nanocrystalline In₂O₃ semiconductor gas sensors, *Sens. Actuators B* 44 (1997) 327–333.
 18. T. Hyodo, H. Inoue, H. Motomura, K. Matsuo, T. Hashishin, J. Tamaki, Y. Shimizu, M. Egashira, NO₂ sensing properties of macroporous In₂O₃-based powders fabricated by

- utilizing ultrasonic spray pyrolysis employing polymethylmethacrylate microspheres as a template, *Sens. Actuators B* 151 (2010) 265–273.
19. P. Sowti Khiabani, A. Hosseinmardi, E. Marzbanrad, S. Ghashghaie, C. Zamani, M. Keyanpour-Rad, B. Raissi, NO₂ gas sensor fabrication through AC electrophoretic deposition from electrospun In₂O₃ nanoribbons, *Sens. Actuators B* 162 (2012) 102–107.
 20. M. Akiyama, J. Tamaki, N. Miura, N. Yamazoe, Tungsten oxide-based semiconductor sensor highly sensitive to NO and NO₂, *Chem. Lett.* 1991 (1991) 1611–1614.
 21. T. Hyodo, Y. Tominaga, T. Yamaguchi, A. Kawahara, H. Katsuki, Y. Shimizu, M. Egashira, NO_x sensing properties of WO₃-based semiconductor gas sensors fabricated by slide-off transfer printing, *Electrochemistry* 71 (2003) 481–484.
 22. J. Tamaki, T. Hashishin, Y. Uno, D. Viet Dao, S. Sugiyama, Ultrahigh-sensitive WO₃ nanosensor with interdigitated Au nano-electrode for NO₂ detection, *Sens. Actuators B* 132 (2008) 234–238.
 23. T. Kida, A. Nishiyama, M. Yuasa, K. Shimano, N. Yamazoe, Highly sensitive NO₂ sensors using lamellar-structured WO₃ particles prepared by an acidification method, *Sens. Actuators B* 135 (2009) 568–574.
 24. E. Comini, G. Faglia, G. Sberveglieri, UV light activation of tin oxide thin films for NO₂ sensing at low temperatures, *Sens. Actuators B* 78 (2001) 73–77.
 25. K. Anothainart, M. Burgmair, A. Karthigeyan, M. Zimmer, I. Eisele, Light enhanced NO₂ gas sensing with tin oxide at room temperature: conductance and work function measurements, *Sens. Actuators B* 93 (2003) 580–584.
 26. J. D. Prades, R. Jimenez-Diaz, F. Hernandez-Ramirez, S. Barth, A. Cirera, A. Romano-Rodriguez, S. Mathur, J.R. Morante, Equivalence between thermal and room temperature UV light-modulated responses of gas sensors based on individual SnO₂ nanowires, *Sens. Actuators B* 140 (2009) 337–341.

27. T. Wagner, C.-D. Kohl, C. Malagù, N. Donato, M. Latino, G. Neri, M. Tiemann, UV light-enhanced NO₂ sensing by mesoporous In₂O₃: Interpretation of results by a new sensing model, *Sens. Actuators B* 187 (2013) 488–494.
28. A. Ilin, M. Martyshov, E. Forsh, P. Forsh, M. Rumyantseva, A. Abakumov, A. Gaskov, P. Kashkarov, UV effect on NO₂ sensing properties of nanocrystalline In₂O₃, *Sens. Actuators B* 231 (2016) 491–496.
29. L. Ding, X. Ding, D. Zeng, S. Tian, H. Li, C. Xie, Visible-light activate mesoporous WO₃ sensors with enhanced formaldehyde-sensing property at room temperature, *Sens. Actuators B* 163 (2012) 260–266.
30. K. Urata, T. Ueda, T. Hyodo, Y. Shimizu, Gas-sensing properties of semiconductor gas sensors operated with UV-light irradiation, *Chem. Sens.*, 30(A) (2014) 109–111.
31. T. Hyodo, K. Urata, T. Ueda, K. Kamada, Y. Shimizu, NO₂-sensing properties of SnO₂-based sensors operated with UV-light irradiation, *Chem. Sens.*, 31(A) (2015) 13–15.
32. F. H. Saboor, T. Ueda, K. Kamada, T. Hyodo, Y. Mortazavi, A. Ali Khodadadi, Y. Shimizu, Enhanced NO₂ gas sensing performance of bare and Pd-loaded SnO₂ thick film sensors under UV-light irradiation at room temperature, *Sens. Actuators B* 223 (2016) 429–439.
33. N. Barsan, U. Weimar, Conduction model of metal oxide gas sensors, *J. Electroceram.* 7 (2002) 143–167.
34. S. Matsushima, T. Maekawa, J. Tamaki, N. Miura, N. Yamazoe, Dispersion and electric interaction of palladium particles supported on tin oxide, *Nippon Kagaku Kaishi* 1991 (1991) 1677–1683.
35. T. Skála, K. Veltruská, M. Moroseac, I. Matolínová, A. Cirera, V. Matolín, Redox process of Pd-SnO₂ system, *Surf. Sci.* 566–568 (2004) 1217–1221.
36. T. Hyodo, T. Yamashita, Y. Shimizu, Effects of surface modification of noble-metal sensing electrodes with Au on the hydrogen-sensing properties of diode-type gas sensors

- employing an anodized titania film, *Sens. Actuators B* 207 (2015) 105–116.
37. M. A. Bulter, D. S. Ginley, Prediction of flatband potentials at semiconductor-electrolyte interfaces from atomic electronegativities, *J. Electrochem. Soc.*, 125 (1978) 228–232.
 38. M. N. Islam, M. O. Hakim, Electron affinity and work function of polycrystalline SnO₂ thin film, *J. Mater. Sci. Lett.* 5 (1986) 63–65.
 39. J. Tauc, R. Grigorovici, A. Vancu, Optical properties and electronic structure of amorphous germanium, *Phys. Status Solidi* 15 (1966) 627–637.
 40. M. Batzill, U. Diebold, The surface and materials science of tin oxide, *Prog. Surf. Sci.* 79 (2005) 47–154.
 41. O. Mounkachi, E. Salmani, H. El Moussaoui, R. Masrour, M. Hamedoun, H. Ez-Zahraouy, E. K. Hlil, A. Benyousse, High blocking temperature in SnO₂ based super-paramagnetic diluted magnetic semiconductor, *J. Alloy. Compd.* 614 (2014) 401–407.
 42. Y. Li, W. Yin, R. Deng, R. Chen, J. Chen, Q. Yan, B. Yao, H. Sun, S.-H. Wei, T/ Wu, Realizing a SnO₂-based ultraviolet light-emitting diode via breaking the dipole-forbidden rule, *NPG Asia Mater.* 4 (2012) e30.
 43. B. Ruhland, T. Becker, G. Müller, Gas-kinetic interactions of nitrous oxides with SnO₂ surfaces, *Sens. Actuators B* 50 (1998) 85–94.
 44. E. P. Gardner, P. D. Sperry, J. G. Calvert, Primary quantum yields of NO₂ photodissociation, *J. Geophys. Res.* 92 (1987) 6642–6652.
 45. O. Lang, C. Pettenkofer, J. F. Sanchez-Royo, A. Segura, A. Klein, W. Jaegermann, Thin film growth and band lineup of In₂O₃ on the layered semiconductor InSe, *J. Appl. Phys.* 86 (1999) 5687–5691.
 46. A. V. Kalinkin, A. M. Sorokin, M. Y. Smirnov, V. I. Bukhtiyarov, Size effect on the oxidation of platinum nanoparticles on graphite with nitrogen dioxide: an XPS and STM study, *Kinet. Catal.* 55 (2014) 354–360.

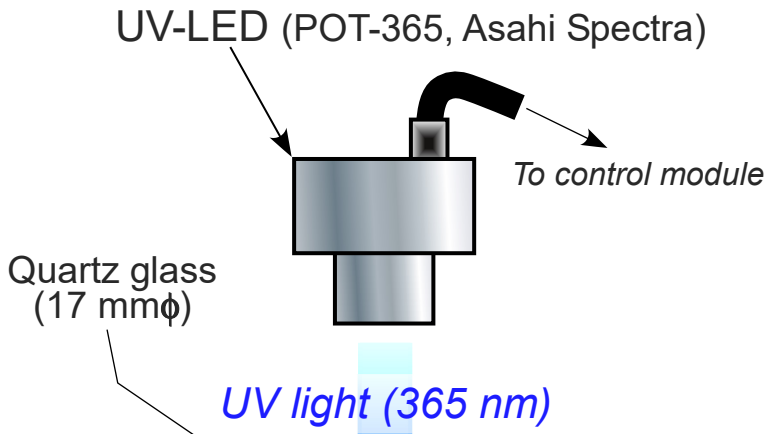
47. N. Ma, K. Suematsu, M. Yuasa, T. Kida, K. Shimano, Effect of water vapor on Pd-loaded SnO₂ nanoparticles gas sensor, ACS Appl. Mater. Inter. 7 (2015) 5863–5869.

Figure Captions

- Fig. 1. Schematic drawing of $0.05\text{Pd}/\text{SnO}_2$ sensor and experimental setup for gas-sensing measurements.
- Fig. 2. Response transients of SnO_2 sensor to 5 ppm NO_2 at 30°C in dry air under different UV-light irradiation intensities.
- Fig. 3. Variations in (a) responses to 5 ppm NO_2 (R_{NO_2}/R_a), (b) resistances in dry air (R_a), and (c) 90% response ($T_{\text{RS}}(90)$, open symbols) and 10% recovery times ($T_{\text{RC}}(10)$, filled symbols) of SnO_2 sensor with UV-light intensity, together with those of In_2O_3 , and WO_3 sensors.
- Fig. 4. Response transients of $0.05\text{Pd}/\text{SnO}_2$ and $0.07\text{Pd}/\text{SnO}_2$ sensors to 5 ppm NO_2 at 30°C in dry air under different UV-light irradiation intensities.
- Fig. 5. Variations in response to 5 ppm NO_2 (R_{NO_2}/R_a) and resistance of all $n\text{Pd}/\text{SnO}_2$ sensors in dry air (R_a) with the amount of Pd loaded, together with those of SnO_2 sensor.
- Fig. 6. XPS spectra of Pd on the surface of $0.05\text{Pd}/\text{SnO}_2$ and $0.10\text{Pd}/\text{SnO}_2$ powders after heat treatment at 500°C for 1 h in ambient air.
- Fig. 7. (a) Representative response transients of SnO_2 and $0.05\text{Pd}/\text{SnO}_2$ sensors to 30% O_2 at 30°C in dry N_2 and (b) variations in response of these sensors to 30% O_2 at 30°C in dry N_2 with UV-light intensity.
- Fig. 8. Diffuse reflectance UV–Vis spectra of (a) SnO_2 and (b) $0.05\text{Pd}/\text{SnO}_2$ powders, together with their Tarc plots.
- Fig. 9. XPS spectra of Pt on the surface of $0.05\text{Pt}/\text{SnO}_2$ and $0.10\text{Pt}/\text{SnO}_2$ powder after heat treatment at 500°C for 1 h in ambient air.
- Fig. 10. Variations in response of $0.05\text{Pt}/\text{SnO}_2$ and $0.10\text{Pt}/\text{SnO}_2$ sensors to 5 ppm NO_2 (R_{NO_2}/R_a) with UV-light intensity, together with those of SnO_2 , $0.05\text{Pd}/\text{SnO}_2$ and $0.10\text{Pd}/\text{SnO}_2$ sensors.

Fig. 11. Variations in response of SnO₂ and 0.05Pd/SnO₂ sensors to 5 ppm NO₂ (R_{NO_2}/R_a) at 30°C in air under UV-light irradiation intensities with relative humidity.

(b) Experimental setup



(a) Sensor element*

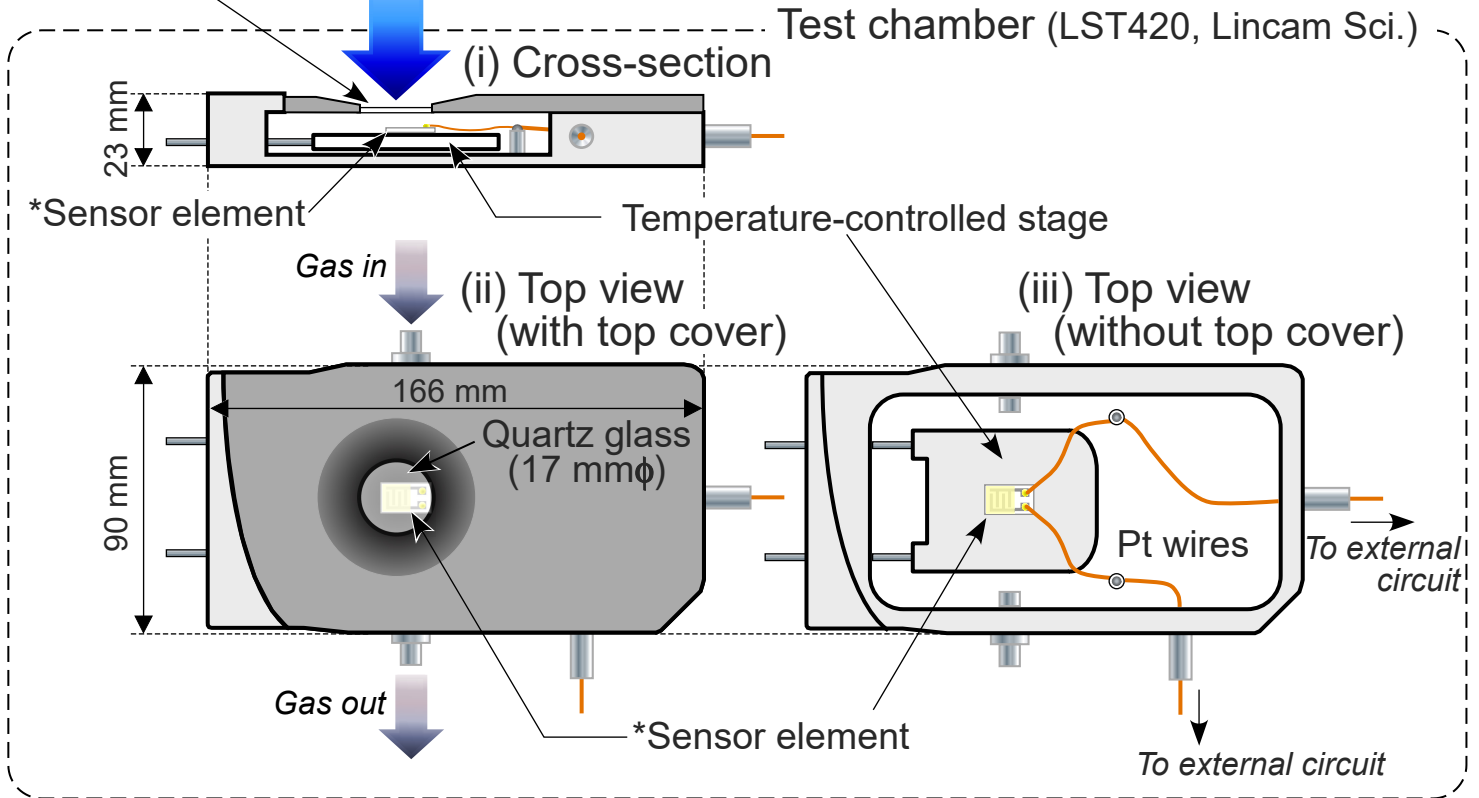
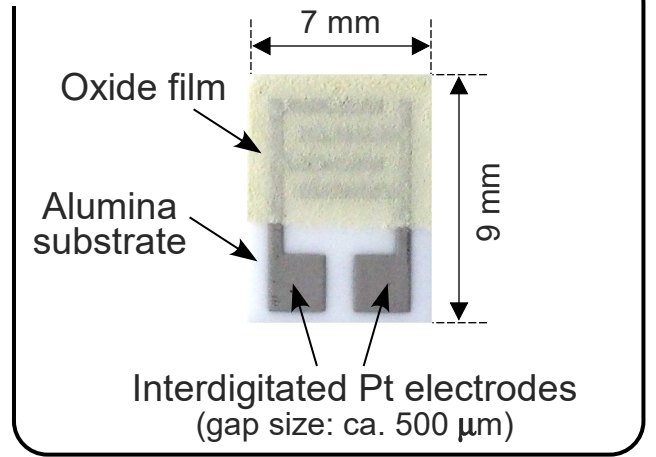


Fig. 1. Hyodo et al.

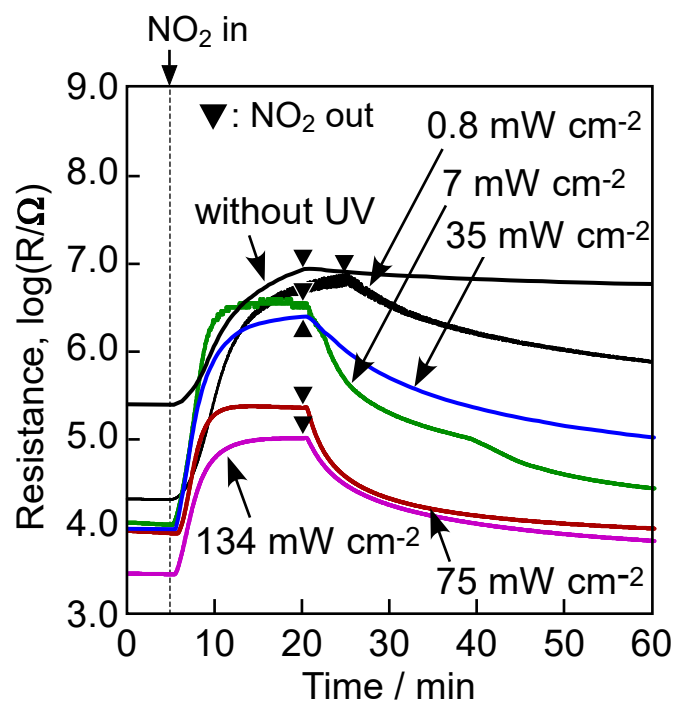


Fig. 2. Hyodo et al.

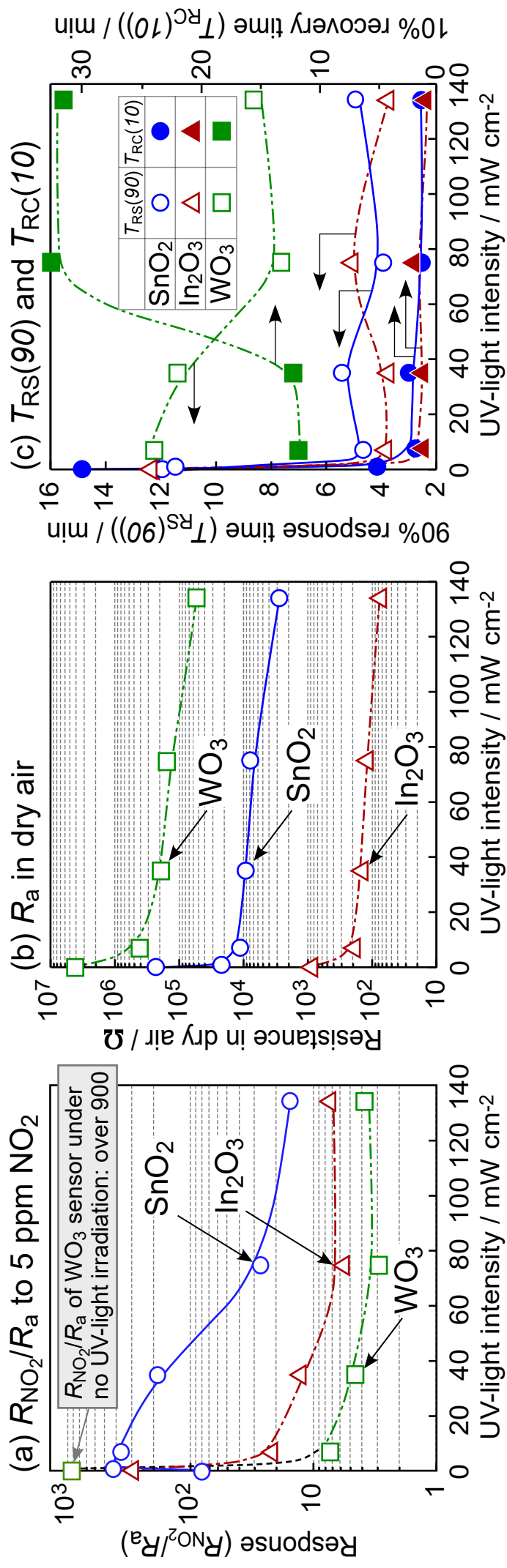


Fig. 3. Hyodo et al.

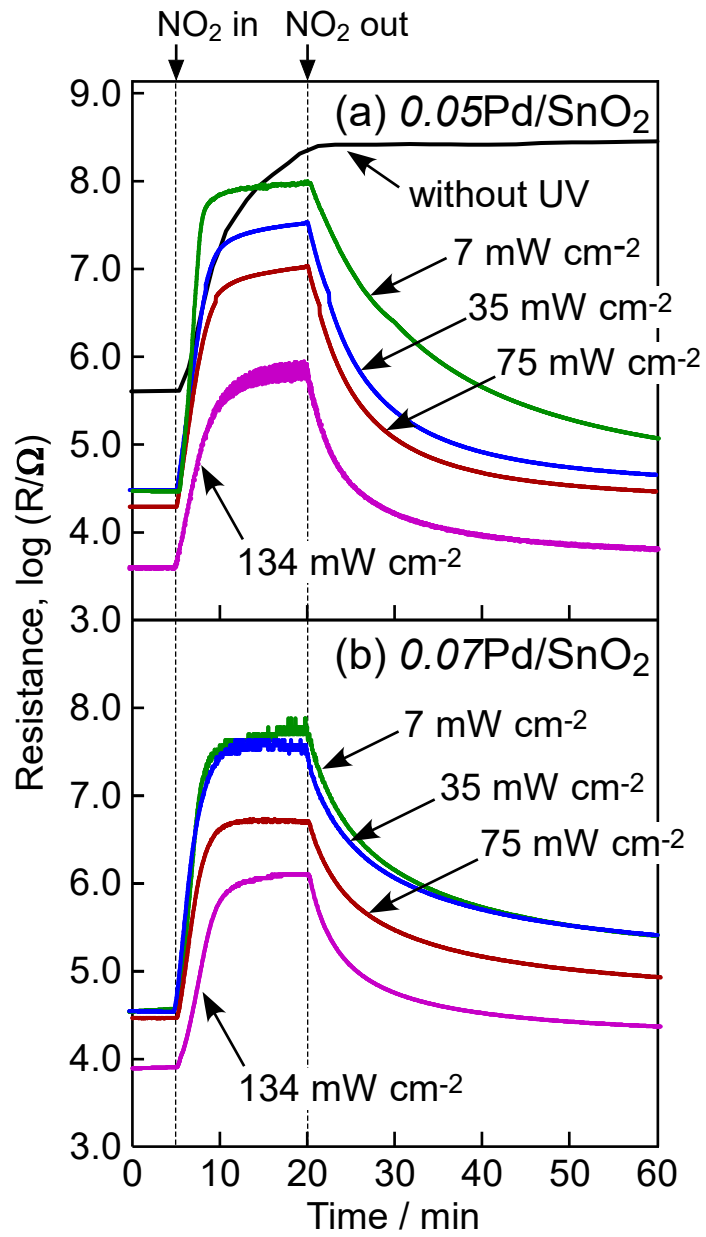


Fig. 4. Hyodo et al.

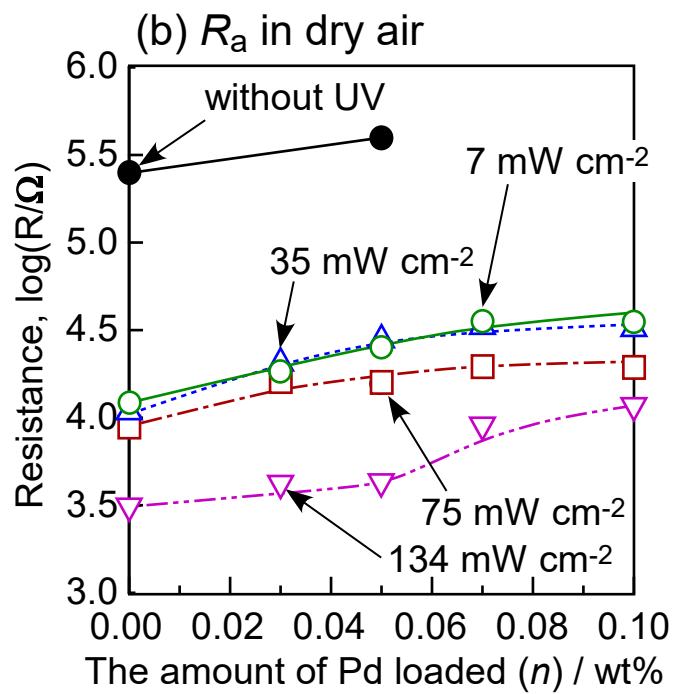
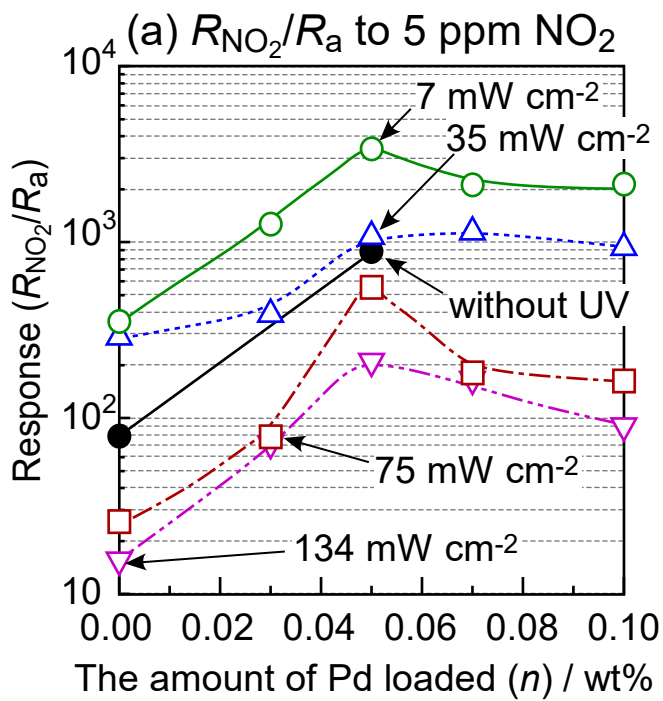


Fig. 5. Hyodo et al.

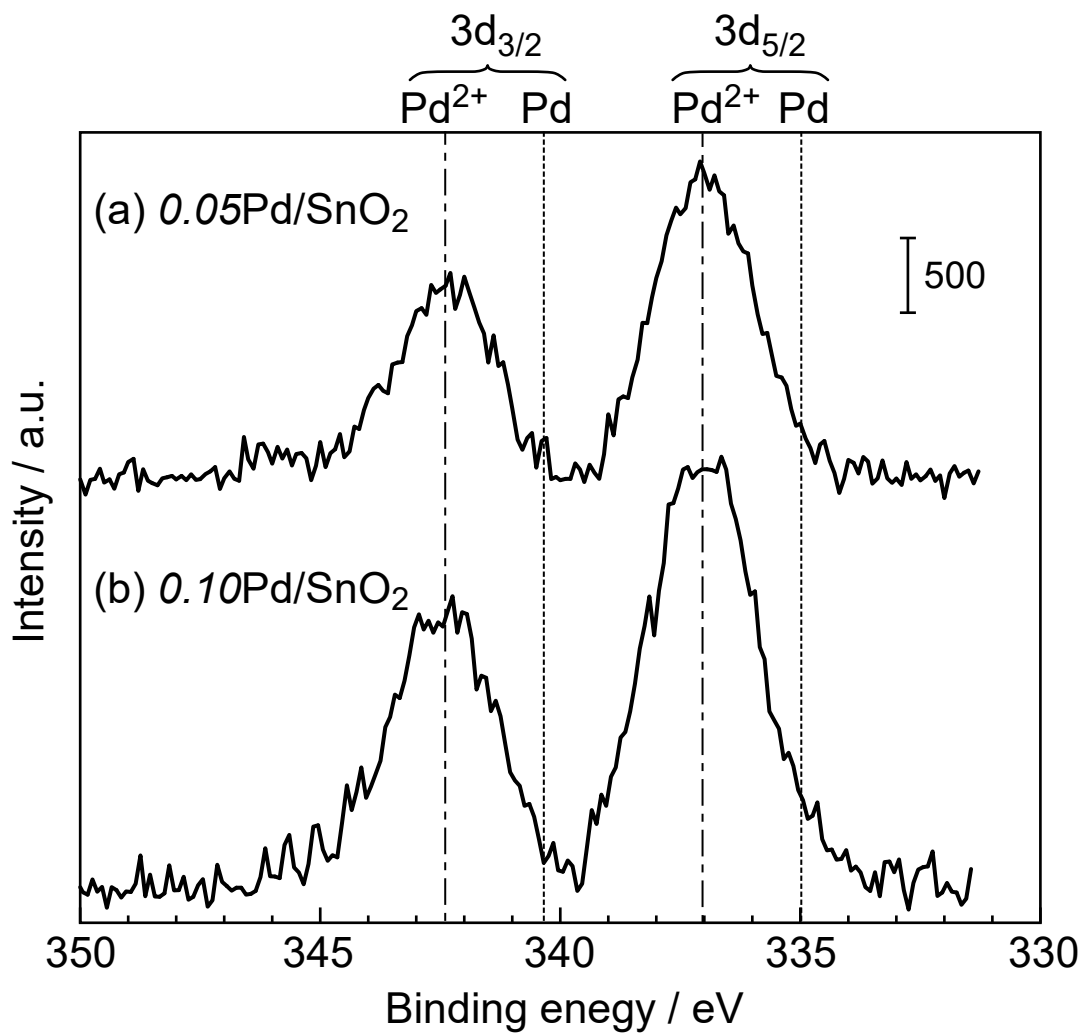
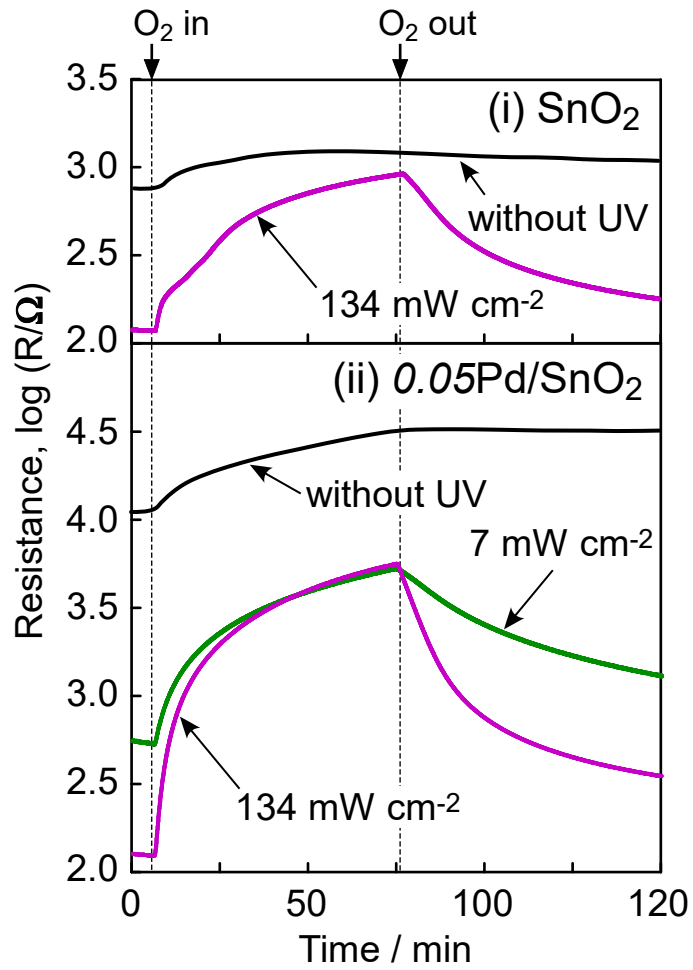


Fig. 6. Hyodo et al.

(a) Response transients



(b) Response to 30% O₂ in N₂

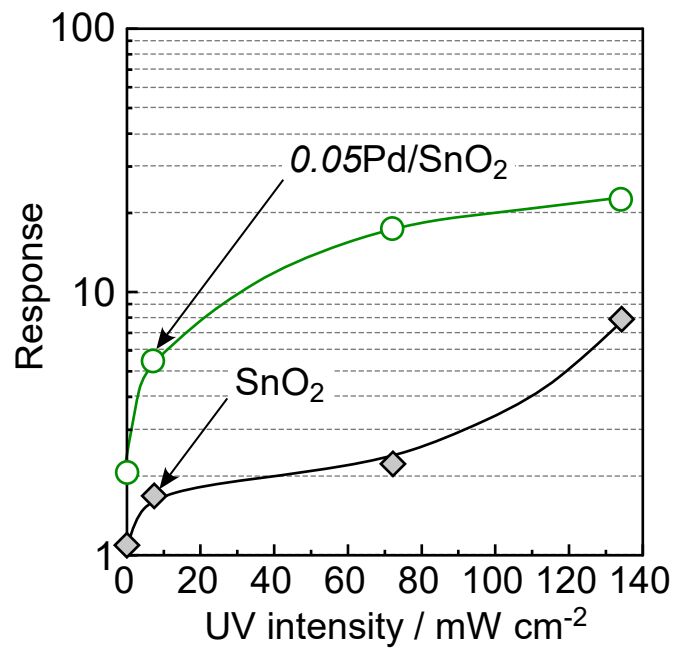


Fig. 7. Hyodo et al.

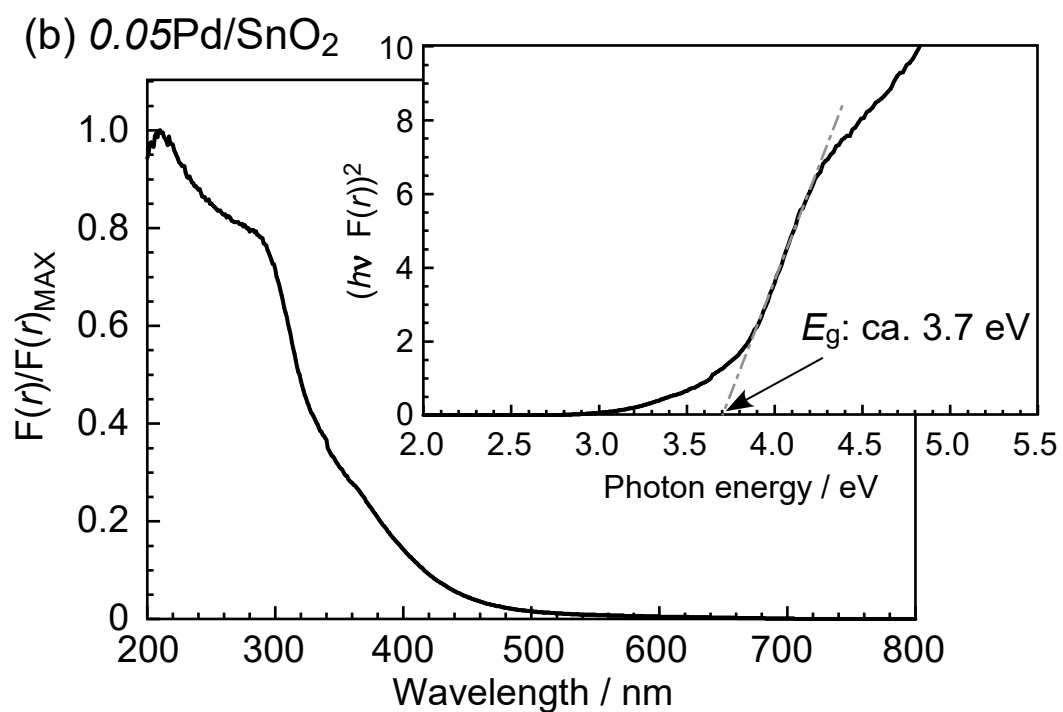
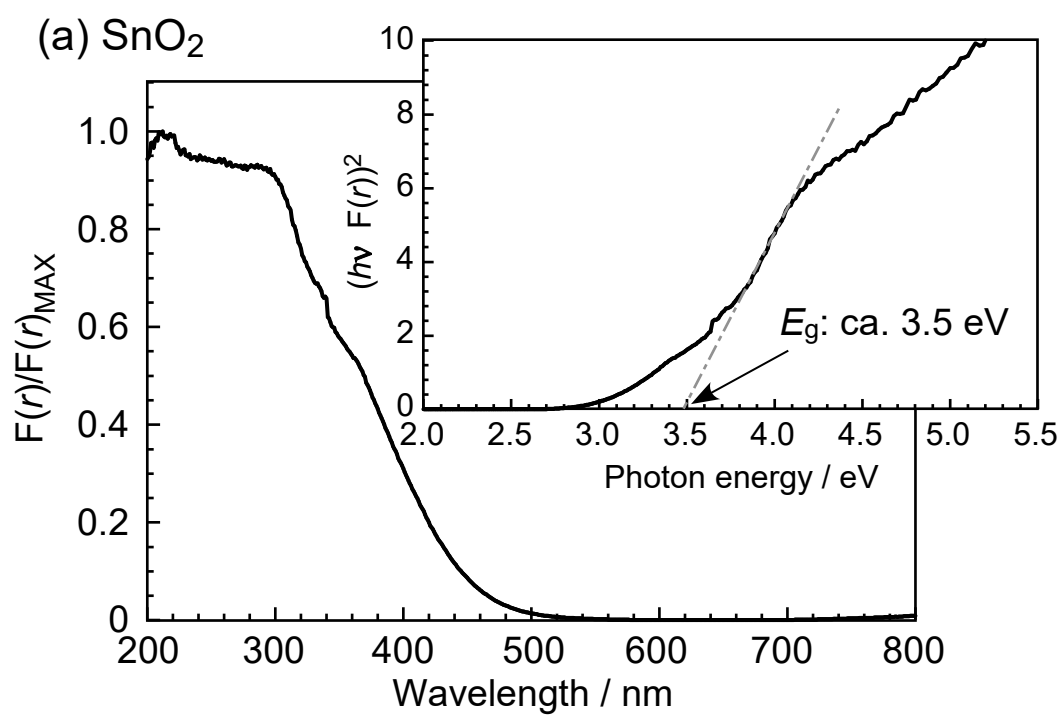


Fig. 8. Hyodo et al.

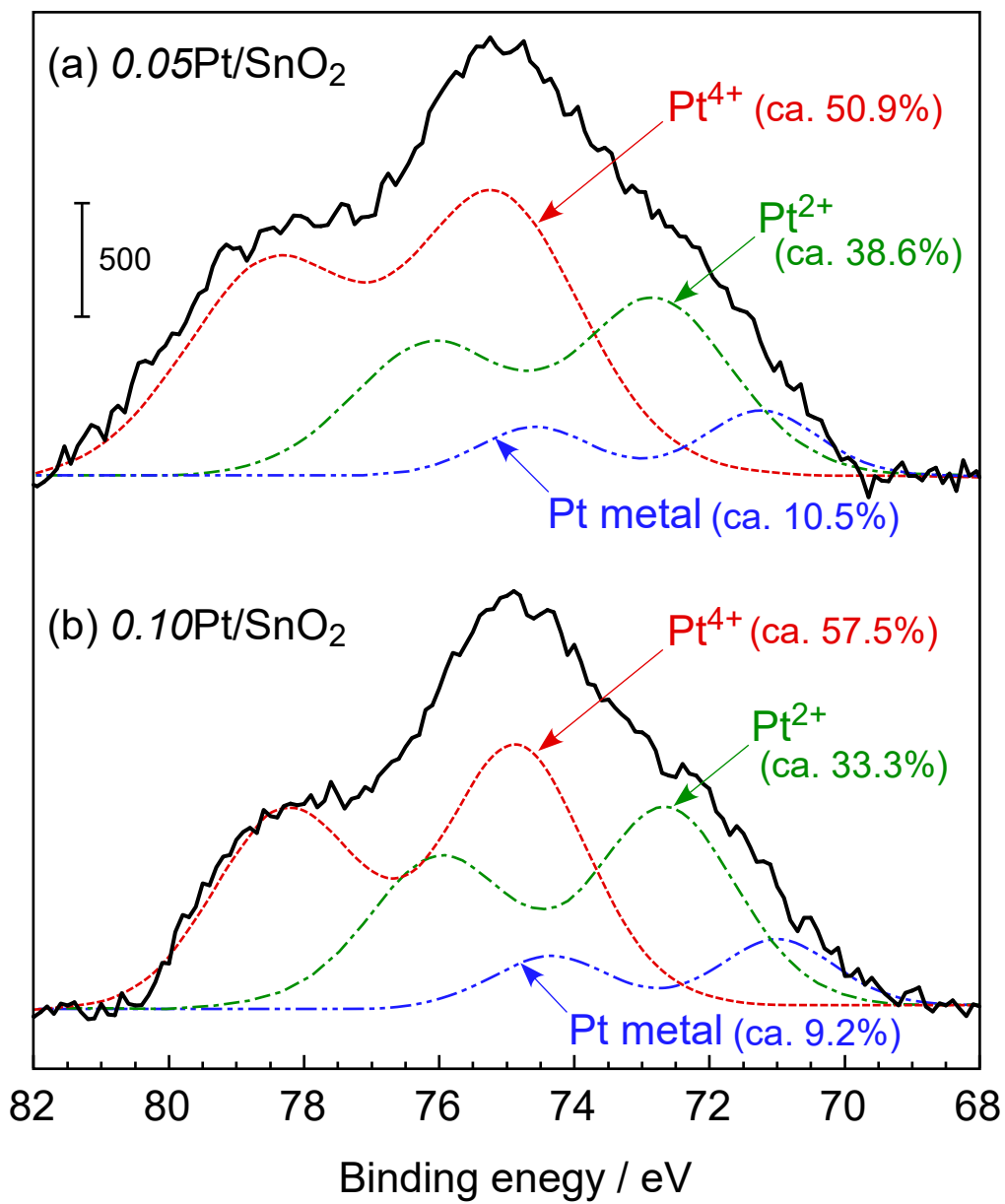


Fig. 9. Hyodo et al.

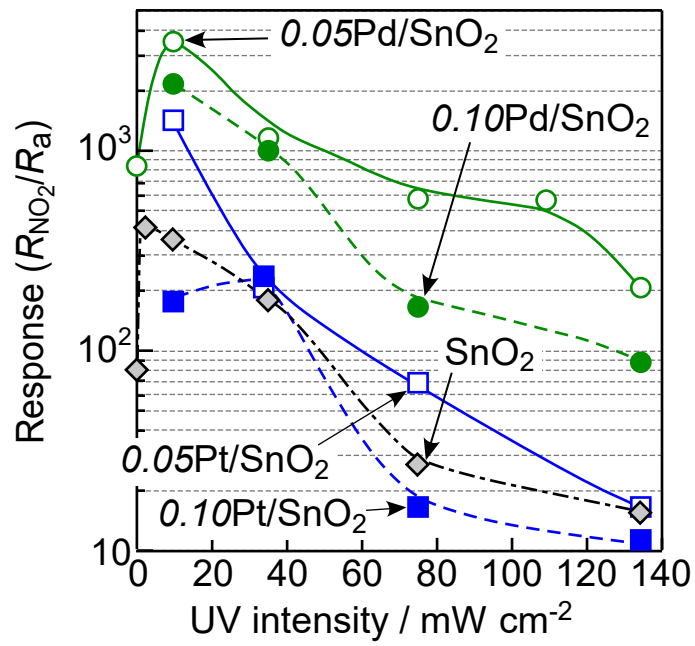


Fig. 10. Hyodo et al.

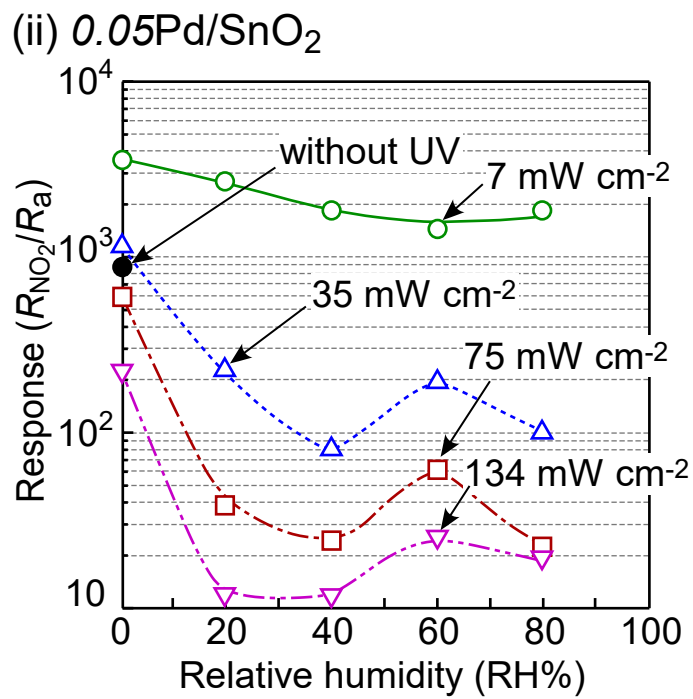
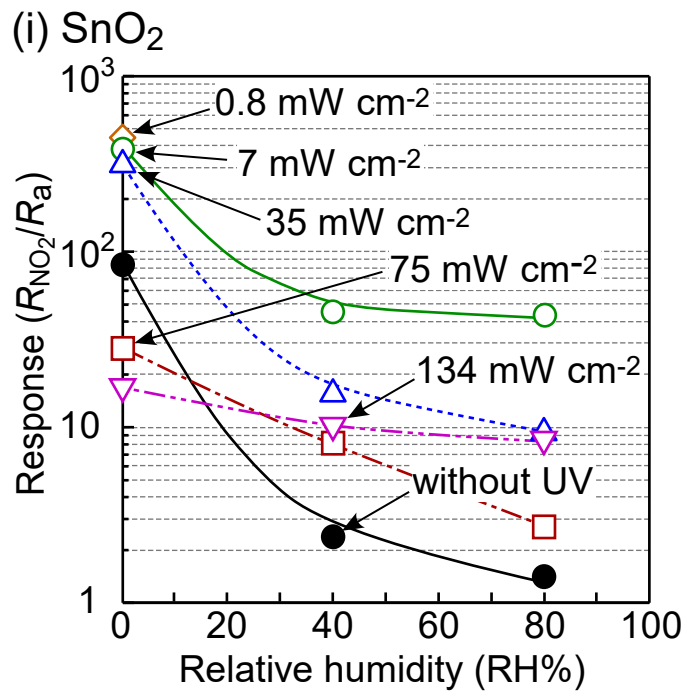


Fig. 11. Hyodo et al.

Supporting Information

Semiconductor-type SnO₂-based NO₂ sensors operated at room temperature under UV-light irradiation

Takeo Hyodo*, Kaoru Urata, Kai Kamada, Taro Ueda, and Yasuhiro Shimizu

Graduate School of Engineering, Nagasaki University
1-14 Bunkyo-machi, Nagasaki 852-8521, Japan

*Corresponding author: hyodo@nagasaki-u.ac.jp

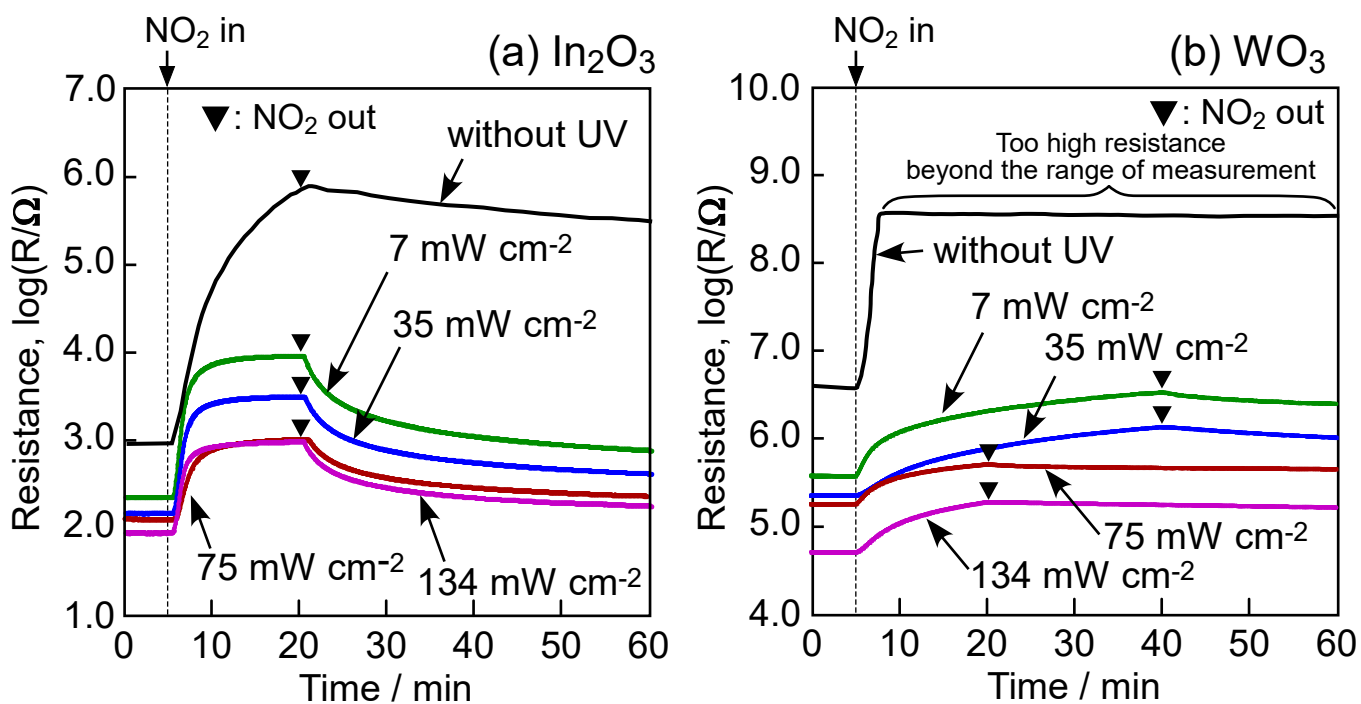


Fig. S1. Response transients of In_2O_3 and WO_3 sensors to 5 ppm NO_2 at 30°C in dry air under different UV-light irradiation intensities.

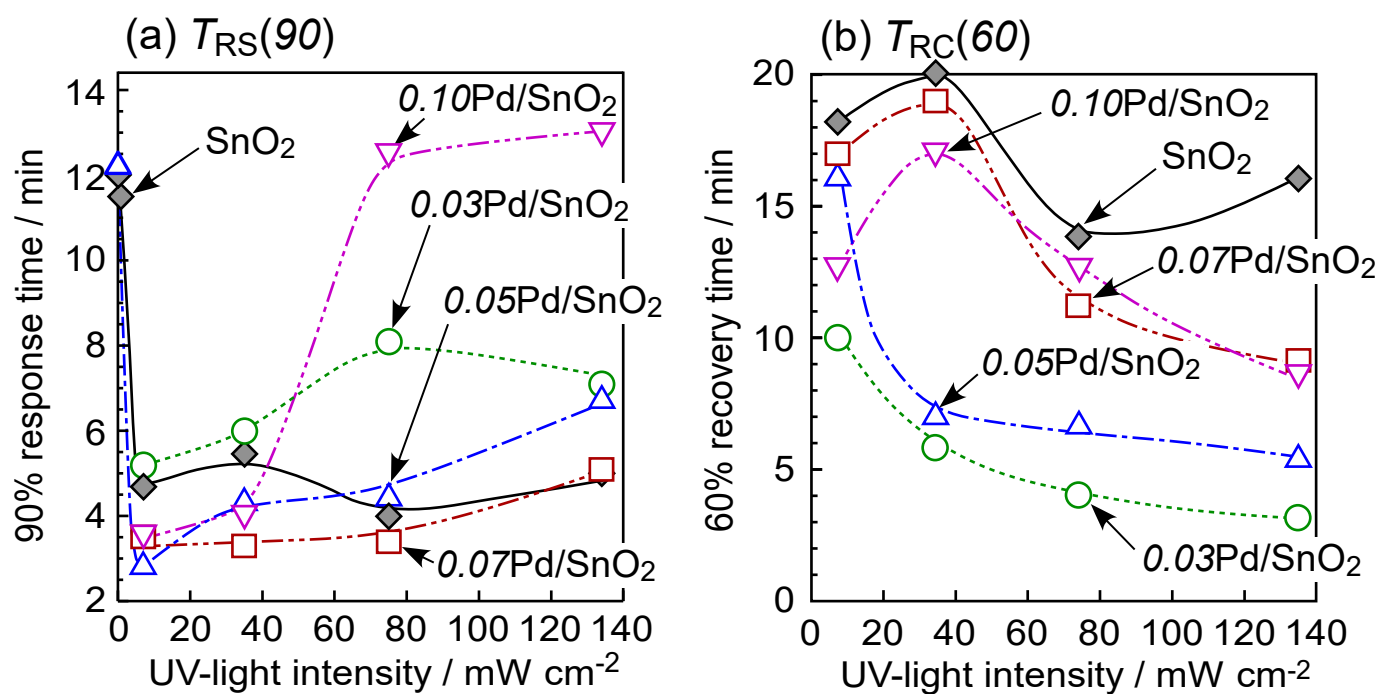


Fig. S2. Variations in 90% response and 60% recovery times ($T_{RS}(90)$ and $T_{RC}(60)$, respectively) of all $n\text{Pd}/\text{SnO}_2$ sensors with UV-light intensity, together with those of SnO_2 sensor.

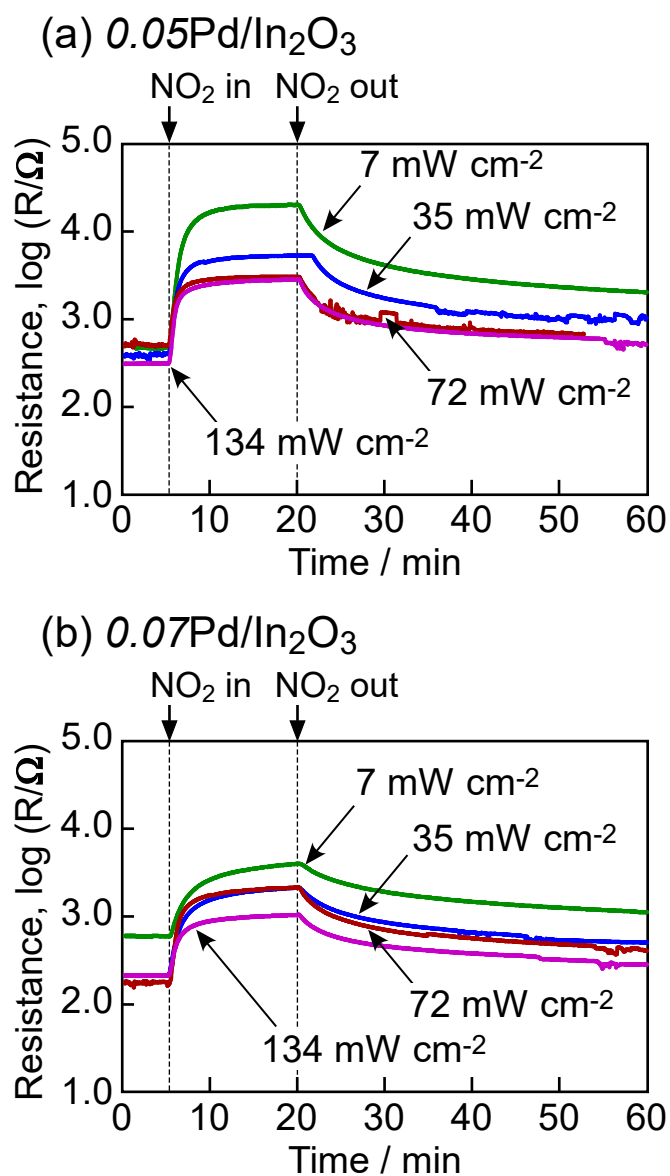


Fig. S3. Response transients of $0.05\text{Pd}/\text{In}_2\text{O}_3$ and $0.07\text{Pd}/\text{In}_2\text{O}_3$ sensors to 5 ppm NO₂ at 30°C in dry air under different UV-light irradiation intensities.

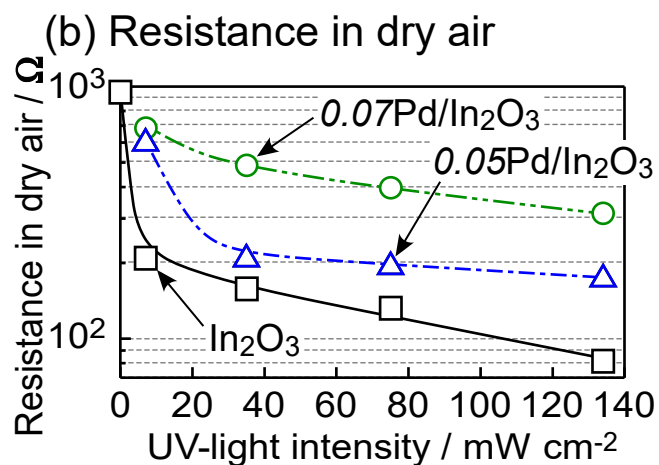
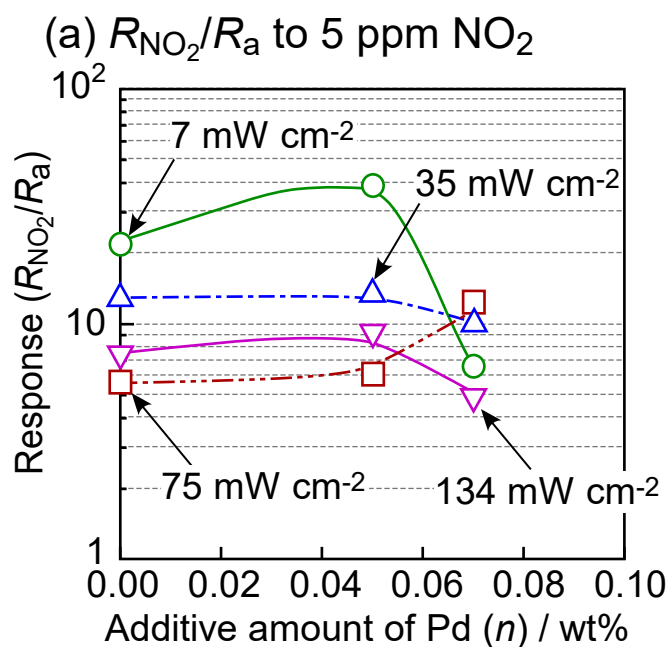


Fig. S4. Variations in response of $0.05\text{Pd}/\text{In}_2\text{O}_3$ and $0.07\text{Pd}/\text{In}_2\text{O}_3$ sensors to 5 ppm NO_2 (R_{NO_2}/R_a) and resistance in dry air (R_a) with the amount of Pd loaded and UV-light intensity, respectively, together with those of In_2O_3 sensor.

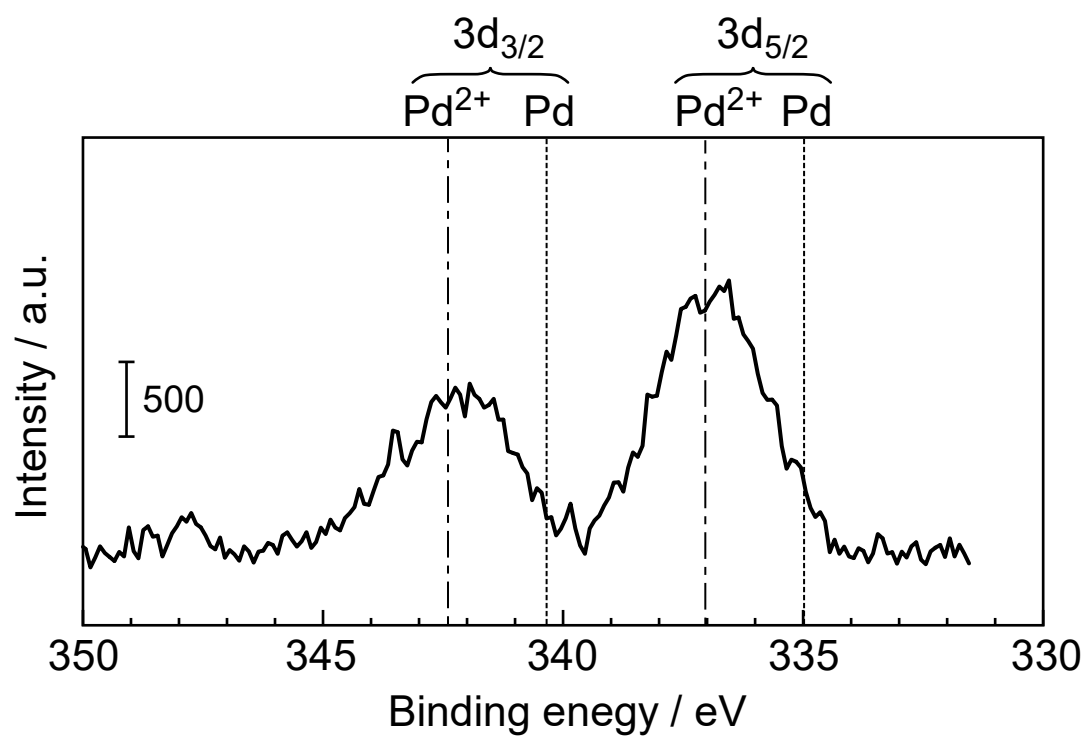


Fig. S5. XPS spectrum of Pd on the surface of $0.07\text{Pd}/\text{In}_2\text{O}_3$ powder after heat treatment at 500°C for 1 h in ambient air.

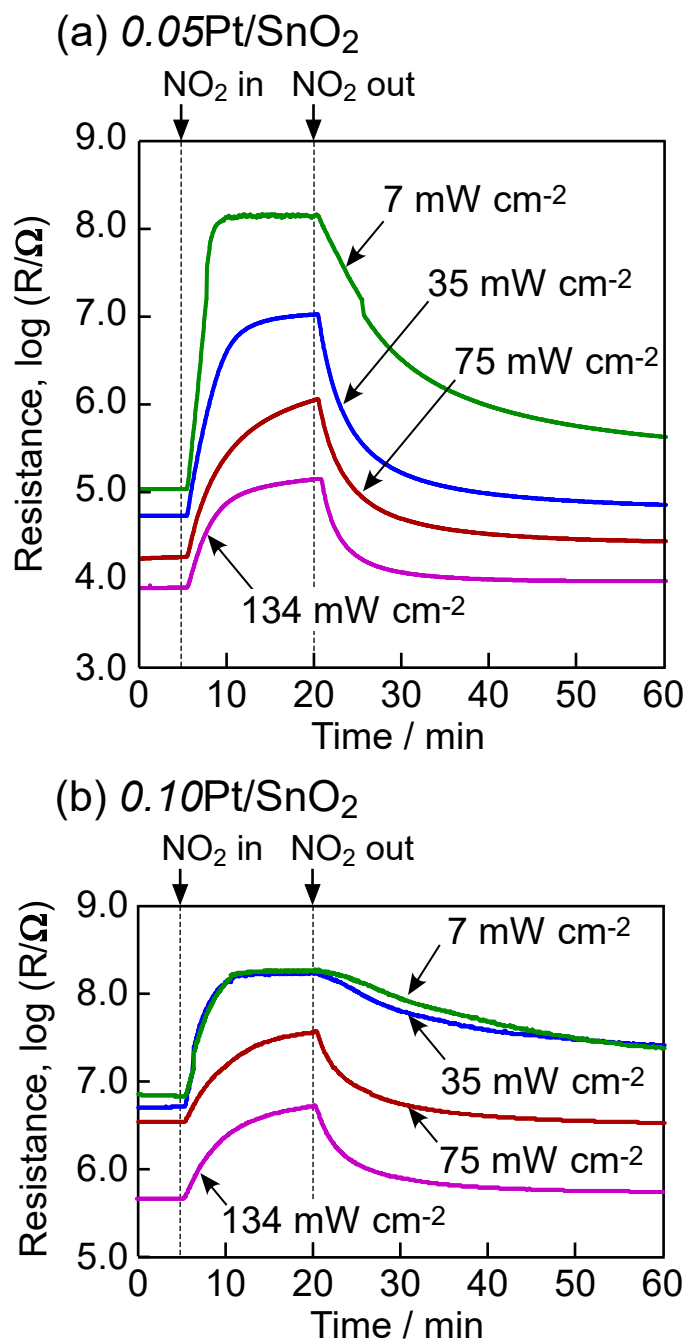


Fig. S6. Response transients of $0.05\text{Pt}/\text{SnO}_2$ and $0.10\text{Pt}/\text{SnO}_2$ sensors to 5 ppm NO₂ at 30°C in dry air under UV-light irradiation.

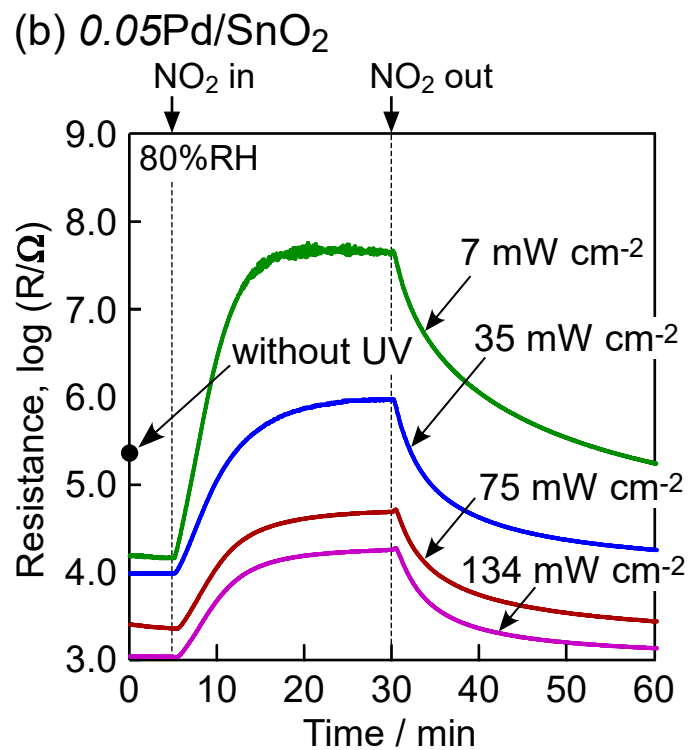
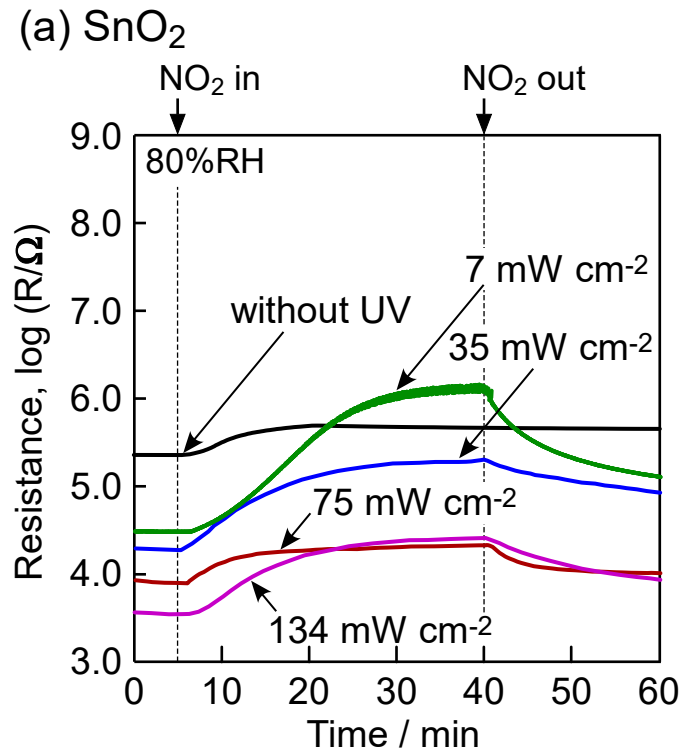


Fig. S7. Response transients of SnO_2 and $0.05\text{Pd}/\text{SnO}_2$ sensors to 5 ppm NO_2 at 30°C in wet air (80%RH) under different UV-light irradiation intensities.